Research article

Facile and green synthesis of recyclable, environmentally friendly, chemically stable, and cost-effective magnetic nanohybrid adsorbent for tetracycline adsorption

Alireza Nasiri [a], Najmeh Golestani [a, b], Saeed Rajabi [a, c, d], Majid Hashemi [a, b, e, *]

[a] *Environmental Health Engineering Research Center, Kerman University of Medical Sciences, Kerman, Iran*
[b] *Department of Environmental Health Engineering, Kerman University of Medical Sciences, Kerman, Iran*
[c] *Student Research Committee, Shiraz University of Medical Sciences, Shiraz, Iran*
[d] *Department of Environmental Health Engineering, School of Health, Shiraz University of Medical Sciences, Shiraz, Iran*
[e] *Student Research Committee, Kerman University of Medical Sciences, Kerman, Iran*

A R T I C L E   I N F O

A B S T R A C T

Antibiotic contamination of water sources, particularly tetracycline (TC) contamination, has emerged as one of the global issues that needs action. In this research, $ZnCoFe_2O_4$@Chitosan (Ch) as a magnetic nanohybrid adsorbent was synthesized using the microwave-assisted co-precipitation method, and their efficiency for the TC adsorption process was investigated. FESEM (Field Emission Scanning Electron Microscope), EDX (Energy Dispersive X-ray), Mapping and line Scan, XRD (X-Ray Diffraction), FTIR (Fourier Transform Infrared Spectrometer), VSM (Vibrating Sample Magnetometer), Thermogravimetric analysis (TGA) and BET (Brunauer Emmett Teller) techniques were used to check and verify its physical and chemical properties. The removal of TC via the adsorption process from synthetic and real wastewater samples was investigated. The factors determining the TC adsorption process, comprising tetracycline concentration (5–30 mg/L), adsorbent dosage (0.7–2 g/L), contact time (2–45 min), and pH (3–11), were evaluated. The removal effectiveness for the synthetic sample and the real wastewater sample was 93 % and 80 %, respectively, under the ideal TC adsorption process parameters of pH 3, adsorbent dosage 1 g/L, TC initial concentration 5 mg/L, and contact time 30 min. According to kinetic and equilibrium studies, the adsorption of TC by $ZnCoFe_2O_4$@Ch follows *pseudo*-second-order kinetics and the Freundlich isotherm. Additionally, it was determined through the analysis of thermodynamic data that the process of exothermic adsorption is spontaneous and is followed by a decrease in disorder ($\Delta H = -15.16$ kJ/mol, $\Delta S = -28.69$ kJ/mol, and $\Delta G = -6.62$ kJ/mol). After five cycles of recovery and regeneration, the $ZnCoFe_2O_4$@Ch magnetic nanocomposite was able to remove 65 % of the TC pollutant and had good chemical stability. The results showed that the magnetic nanoadsorbent $ZnCoFe_2O_4$@Ch is a novel magnetic nano-adsorbent with high adsorption capacity that can be utilized to eliminate pharmaceutical contaminants from aqueous solutions.

---

* Corresponding author. Environmental Health Engineering Research Center, Department of Environmental Health, Kerman University of Medical Sciences, Kerman, Iran.
E-mail addresses: mhashemi120@gmail.com, ma.hashemi@kmu.ac.ir (M. Hashemi).

1. Introduction

The discharge of industrial effluents comprising organic and inorganic chemicals into environments is one of the foremost noteworthy sources of contamination. Pharmaceutical products are among the persistent pollutants in wastewater, and the prevalence of various pharmaceutical product subgroups in aquatic environments has drawn more attention [1–5]. In common, there are numerous diverse ways that pharmaceutical products are presented into the environment, including rural runoff, coordinated release from civil and healing center wastewater treatment facilities, coordinated release of therapeutic, veterinary, and industrial waste, and dumping of expired pharmaceutical products [6]. Low concentrations of antibiotics will cause antibiotic resistance and in high concentrations, the compounds are toxic to microorganisms. Although these substances only exist in extremely small amounts in water nanograms or micrograms per liter-their accumulation in plants, animals, and humans can eventually harm live organisms [7]. Antibiotics are a type of medicine that is frequently used in human societies to both prevent and cure bacterial infections. Some of these substances' metabolites are eliminated from the body and discharged into the environment because the human body cannot fully metabolize them. This increases the requirement to recognize and eliminate these substances from aquatic habitats and water supplies [6].

Tetracyclines (TC) are broad-spectrum antibiotics with $C_{22}H_{24}N_2O_8$ molecular formula used to treat gram-positive and gram-negative bacteria as well as intracellular chlamydia, mycoplasma, and rickettsia and it is regarded as the second-most utilized antibiotic in the world due to benefits including lower prices and better antibacterial activity [8]. Tetracycline concentrations are estimated to be 15 µg/L in surface and groundwater, 86–199 µg in soil, 4 µg/L in liquid fertilizers, and 3 µg/L in wetlands [9]. On the other hand, antibiotics can produce undesirable byproducts when water is chlorinated and ozonated in a wastewater treatment facility [10]. Therefore, it is necessary to purify water and wastewater that contain TC antibiotic before releasing them into the environment.

The removal of antibiotics from wastewater can be accomplished in a variety of methods, including physical, chemical, and biological [11,12]. The method chosen will depend on the chemical and physical properties of the material, the required efficiency, and the planned use of the treated effluent [13,14]. These techniques consist of ultraviolet photolysis [15], surface adsorption [16–18], biodegradation [19], photocatalytic degradation [20,21], advanced oxidation processes during Fenton processes [22], photo-Fenton [23], electro-Fenton [24], photo-electro-Fenton [25], ozonation [26], immobilization of catalytic degrading enzyme [27], and catalytic ozonation [28]. Despite the benefits, each of these techniques also has drawbacks that frequently make it challenging to employ them.

The adsorption process is a promising method for reducing pollutants due to its low operating costs, high flexibility, non-sensitivity to toxic compounds and contaminants, lack of secondary pollution in the system, possibility of adsorbent separation, effectiveness, and high specific surface area for removal of pharmaceutical products [29], dye compounds [30], and heavy metals [31]. The majority of solid porous adsorbents used in adsorption operations have pores that are in the nanoscale range [32]. Nanomaterials' large surface area and the presence of active sites give them a great capacity for adsorption [33]. Additionally, magnetic nanosorbents can be separated and reused afterward [34].

The development and synthesis of magnetic adsorbents, iron oxides, and other ferrite compounds have drawn a lot of interest [35–39]. Due to their excellent adsorption effectiveness, cheap production cost, quick separation, low pollutant generation, and higher treatment efficiency in a short amount of time, magnetic adsorbents have found a good role in the treatment of water and wastewater [40]. MOF@GO [41], SF-Fe$_3$O$_4$-EDTA [42], CoFe$_2$O$_4$@γ-Fe$_2$O$_3$ [43], Thioglycolic-modified Zn–Fe layer double hydroxide [44], CoFe$_2$O$_4$@SiO$_2$–C$_8$ [45], GO/g–C$_3$N$_4$–Fe$_3$O$_4$ [46], Fe$_3$O$_4$@SiO$_2$@CS/GO [47], Ni/HAP/CoFe$_2$O$_4$ [48], and AC-Fe$_3$O$_4$ [49] are different magnetic nanosorbents that have been applied thus far.

In order to enhance the structure and function of these magnetic nanosorbents, biological substances can be used in their synthesis [36,37,50]. Chitin is used to produce the natural amino polysaccharide known as chitosan (Ch) [51,52]. Following cellulose, chitin is the second most prevalent polymer in nature. It may be taken from the shells of many crustaceans, including insects, fungi, and shrimp. Due to its unique qualities, including hydrophilicity, biocompatibility, biodegradability, non-toxicity, and most crucially the characteristics of high adsorption in the synthesis of nanosorbents, chitosan should be employed as a biopolymer [53].

Cellulose-derived carbohydrate biopolymers have a wide range of uses in water and wastewater treatment procedures because they are biodegradable, affordable, readily accessible, regenerative, stable, non-toxic, and have a high permeability. By magnetizing these polymeric carbohydrates and synthesizing ferrite nano-biocomposites, lumpy and low surface area issues can be resolved.

In the adsorbent structure, metal ions of transition metals including cobalt, zinc, and iron can function as either Lewis's acids or electron receptors. Functional groups in the TC structure like hydroxyl, amine, and carbonyl may also act as electron donor groups (EDGs) for transition metals such as cobalt, zinc, and iron. The EDGs of TC interact with the metal ions of the transition metals as electron-withdrawing groups (EWGs) to form a complex between the TC and the adsorbent. This complex's formation could affect the TC adsorption procedure [54,55].

In this research, a new magnetic material called ZnCoFe$_2$O$_4$@Ch was made using a biopolymer called Ch. It can be used to remove TC from water. Adding Ch during the making of ZnCoFe$_2$O$_4$@Ch makes the magnetic material have a bigger surface area. Furthermore, the amine and hydroxyl groups in Ch create a strong pull towards the adsorbent surface. This means that more TC molecules stick to the ZnCoFe$_2$O$_4$@Ch surface and interact with it, which helps the adsorption process. Also, we looked at how different factors like the acidity of the solution, the amount of TC in the beginning, the amount of adsorbent used, and how long they were in contact, affected how well the adsorbent worked. We also studied how quickly the adsorbent worked and the energy involved in the process. The reusability and chemical stability of nano-biocomposite were also assessed.

2. Materials and methods

2.1. Chemicals

Cobalt (II) chloride hexahydrate (CoCl$_2$·6H$_2$O), iron (III) chloride hexahydrate (FeCl$_3$·6H$_2$O), zinc chloride (ZnCl$_2$), sodium hydroxide (NaOH), chitosan (Ch) and hydrogen chloride (HCl) were purchased by Sigma Aldrich and Merck companies. The tetracycline was provided by Darou Pakhsh Pharmaceutical Manufacturing Company (Tehran, IRAN). Deionized water was used to make the experiment solutions. HCl and NaOH (1 *N*) were used to alter the pH of the solutions.

2.2. Characterizations

A microwave oven (SAMSUNG, 2450 MHz, 800 W) was applied to synthesize the magnetic nano adsorbent. XRD to determine the magnetic nano-crystal adsorbent's structure and phase (PHILIPS PW1730), FESEM to investigate the structure, composition, and surface structure of magnetic nano-adsorbents on the nanoscale (TESCAN MIRA III), EDX, Mapping and Line scan to investigate the element weight percentages, types, and distributions at the surface of magnetic nano-adsorbent (TESCAN MIRA II, SAMX Detector), FTIR to investigate chemical bonding in magnetic nano-adsorbents and determine functional groupings (AVATAR, Thermo), VSM to determine the magnetic properties of magnetic nano-adsorbent (LBKFB, Kashan Kavir Magnet Company), TGA (SDT, Q600) to determine the adsorbent's thermal stability, and BET to determine the size of a magnetic nano adsorbents specific region (BELSORP MINI II), techniques were used to study the structure of the resultant adsorbent. After confirming the magnetic nano adsorbent's physical and chemical structure, it was used to adsorb TC from an aqueous medium. A UV–vis spectrophotometer (SHIMADZU, UV-1800) was applied to detect the concentration of TC at a maximum wavelength of 357 nm (λ_{max} = 357 nm).

2.3. Preparation of ZnCoFe$_2$O$_4$@Ch

ZnCoFe$_2$O$_4$@Ch nanocomposite was synthesized by modifying previously reported methods [56,57]. Stoichiometric amounts of metal chlorides (5.4 g FeCl$_3$·6H$_2$O, 1.2 g CoCl$_2$·6H$_2$O, and 0.7 g ZnCl$_2$) and chitosan (1 g) were respectively dissolved in 100 mL of deionized water. Then 6 g of NaOH was gradually added to the mixture over the course of an hour to alkalize the pH of the solution. Then the resulting mixture was placed in the microwave at 450-W 3 times for 5 min to obtain a black precipitate. The resulting sediment was separated using a magnet and rinsed several times with deionized water to neutralize the final pH. Eventually, the black precipitate was dried for 24 h at 70 °C temperature (in the furnace).

2.4. Batch adsorption experiments

At first, TC stock solution was prepared with a concentration of 100 mg/L and then concentrations of 10, 15, 20, 30, and 40 mg/L were prepared from it. To optimize the adsorbent dose, amounts of (0.7, 1, 1.5, 2) g/L were investigated. Solutions of 1 *N* NaOH and HCl were used to adjust the pH and pHs of 3, 5, 7, 9, and 11 were investigated. Contact times of 45 min and temperatures of 25, 35, 45, and 55 °C were investigated and optimized. Fig. 1 shows the batch adsorption setup schematic. All the experiments were performed on the synthetic samples. ZnCoFe$_2$O$_4$ alone and Ch alone were utilized as the controls to assess the superior performance of ZnCo-Fe$_2$O$_4$@Ch magnetic nanocomposite. After optimizing the adsorption process conditions on the synthetic samples, the TC adsorption
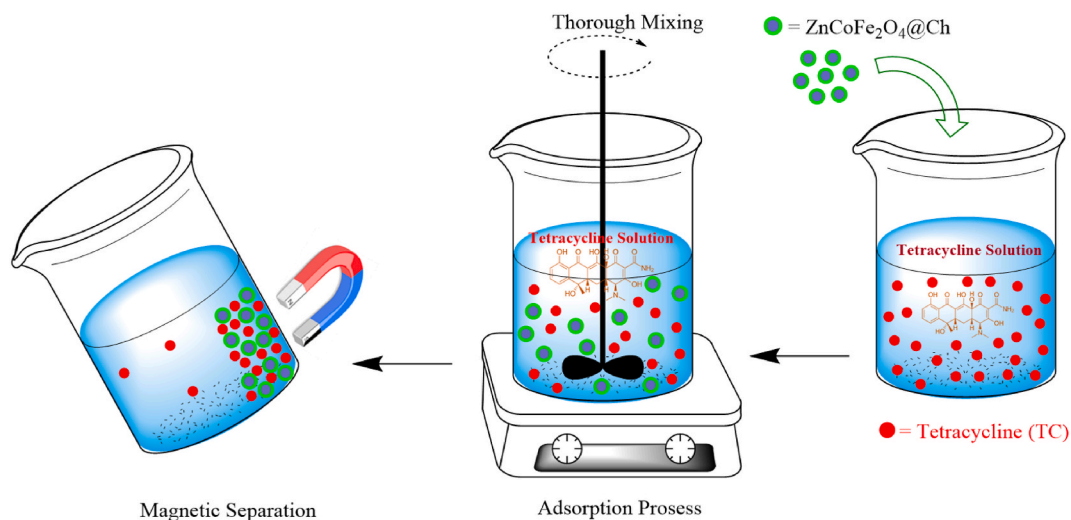
Fig. 1. Batch adsorption process setup schematic.

process has been carried out under optimal conditions on the Kerman University of Medical Sciences (Kerman, IRAN) with coordinates $30°.24'$ latitude and $57°.10'$ longitude wastewater sample as a real sample.

Finally, the adsorption efficiency (Eq. (1)) and adsorption capacity (Eq. (2)) were calculated by the following equations [58]:

$$R_e \ (\%) = \frac{C_0 - C_t}{C_0} \times 100 \qquad \qquad \text{(Eq. 1)}$$

R_e: adsorption efficiency (%)
C_0 and C_t: initial concentration and final concentration (mg/L) of TC, respectively.

$$Q_e = \frac{(C_0 - C_t)V}{m} \qquad \qquad \text{(Eq. 2)}$$

Q_e: adsorption capacity
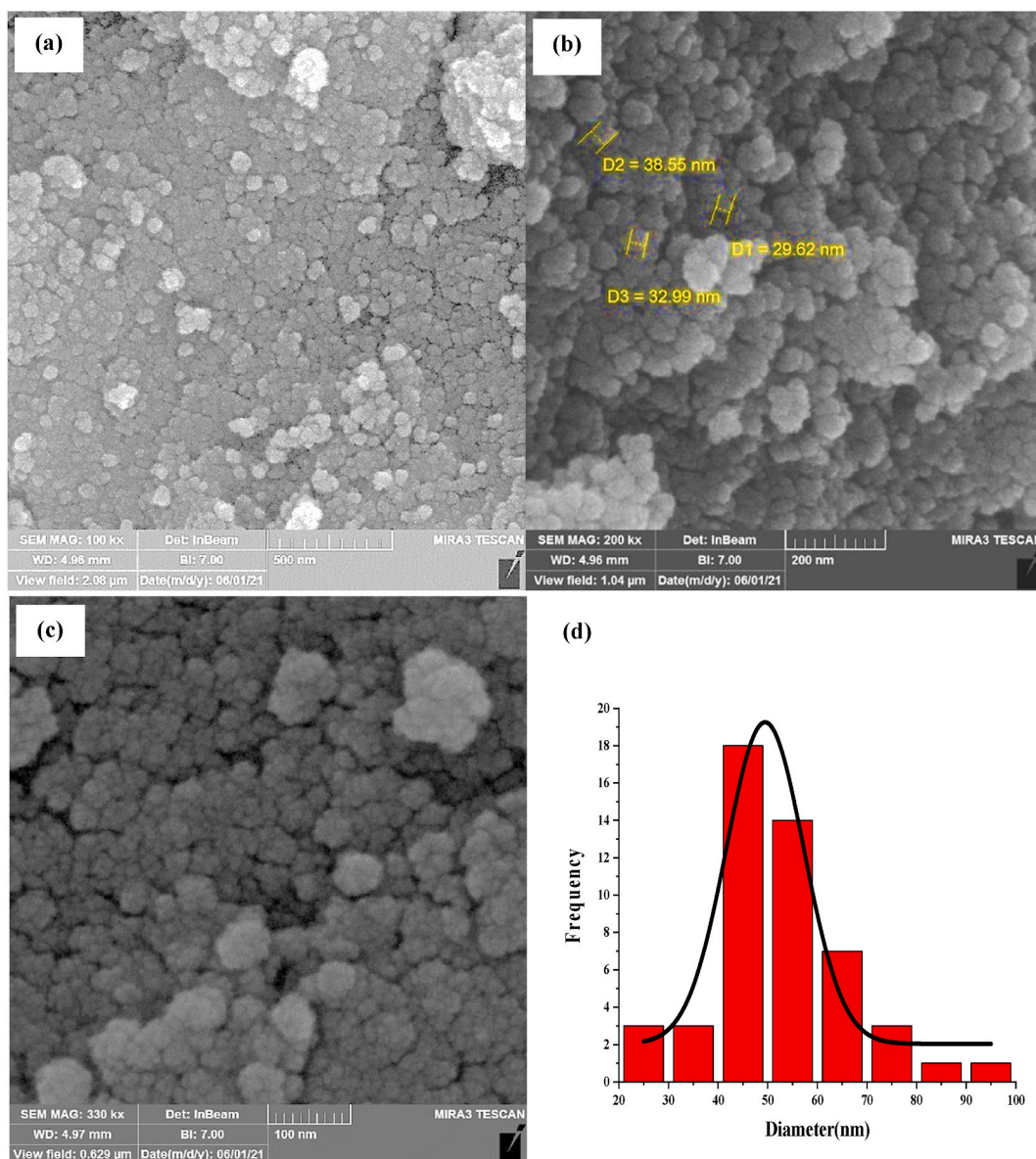
Fig. 2. FESEM images of ZnCoFe$_2$O$_4$@Ch magnetic nanoadsorbent with 500 nm (a), 200 nm (b), 100 nm (c) magnification and particle size distribution (d).

V: volume of solution (L)

m: adsorbent mass (g).

2.5. Determination of pH_{zpc}

To calculate the pH_{zpc}, first, 300 mL of KCl solution (0.1 M) was prepared with distilled water. Then the prepared solution was divided into six 50 mL containers. In each container, 0.01 g of nano-adsorbent was added after the pH of the solutions was adjusted to 2, 4, 6, 8, 10, and 12. The ultimate pH of these solutions was measured after they had been shaken on the shaker for 24 h. The intersection of ΔpH with the X axis, which was determined by drawing a graph of ΔpH (the difference between primary and secondary pH), and initial pH, was determined to be pH_{zpc} [7].

3. Results and discussion

3.1. Characterization of the synthesized magnetic nano adsorbent

Initially, the novel magnetic nano adsorbent $ZnCoFe_2O_4@Ch$ was prepared from Zn^{2+}, Co^{2+}, and Fe^{3+} in the presence of chitosan by using a microwave-assisted technique based on the experimental procedure. To characterize this magnetic nano adsorbent, several techniques were applied. To determine the shape and size, the FESEM images of the produced $ZnCoFe_2O_4@Ch$ were illustrated. Fig. 2 (a–c) depict the FESEM images of $ZnCoFe_2O_4@Ch$ synthesized in the presence of chitosan as a polysaccharide. As evident from the figure, the magnetic nanoadsorbent formed in the presence of chitosan exhibited loosely aggregated, evenly distributed, and gently rounded morphology. Fig. 2d shows the particle size distribution. From the particle size distribution histogram, it can be concluded that the average particle size of magnetic nano adsorbent is 40–50 nm. Rahmi et al. also synthesized nanocomposites in the presence of chitosan, which was highly efficient in removing cadmium. They discovered that the syringe-drop-wising procedure was mostly responsible for influencing the form of nanoparticles. Further evidence for an equitable distribution of Fe_3O_4 was provided by the presence of particle-like fillers that covered the whole surface of the bead [59–61].

The purity and chemical structure of synthesized $ZnCoFe_2O_4@Ch$ were evaluated by EDS analysis (Fig. 3). The EDS results demonstrate 44.24 % O, 27.33 % Fe, 8.13 % C, 7.75 % Co, 7.25 % Zn, and 5.31 % N in the chemical structure of $ZnCoFe_2O_4@Ch$ magnetic nano adsorbent which are following the expected values.

Mapping was used to investigate the $ZnCoFe_2O_4@Ch$ magnetic nano adsorbents element distribution (Fig. 4a). The green, blue, purple, turquoise, red, and yellow spots in Fig. 4 illustrate the distribution of elements on the surface of nanoparticles; these hues correspond to the elements oxygen, nitrogen, iron, cobalt, carbon, and zinc, respectively. Based on the obtained results, Co, Fe, O, N, Zn, and C had a homogeneous distribution that indicated high uniformity of the synthesized $ZnCoFe_2O_4@Ch$. Also, line scanning shown in Fig. 4b has confirmed these results.

Fourier transform infrared spectroscopy (FTIR) has been used to identify the functional group of synthesized nanoparticles. By using a KBr disc, the powdered $ZnCoFe_2O_4@Ch$ was investigated (Fig. 5). In the FTIR spectrum, chitosan absorption bands are shown (Fig. 5). The stretching vibrations of the hydroxyl group O–H are responsible for the absorption band in the 3418 cm^{-1} range. The stretching vibrations of the C–H group are associated with the absorption band in the range of 2866 cm^{-1}. The bending vibrations of the primary amine group NH_2 and the stretching vibrations of the C–O alcoholic group were observed in the range of 1621 cm^{-1} and 1160 cm^{-1}, respectively. In the ranges of 1121 cm^{-1} and 2001 cm^{-1}, respectively, ethereal C–O stretching vibrations and C–N stretching vibrations were seen [62–64]. Additionally, according to the FTIR spectra, the absorption bands for $ZnCoFe_2O_4@Ch$

Elements	W%
O	44.24
Fe	27.33
C	8.13
Co	7.75
Zn	7.25
N	5.31
Total	100.00
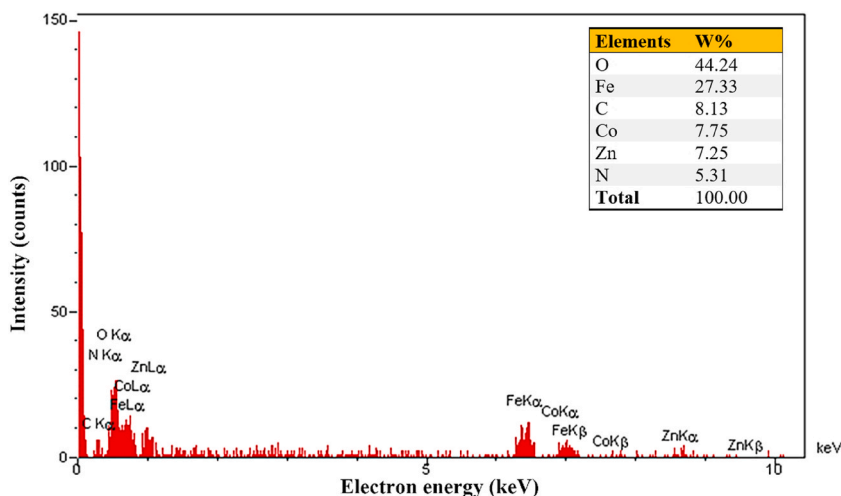
Fig. 3. EDS of $ZnCoFe_2O_4@Ch$ magnetic nanoadsorbent.
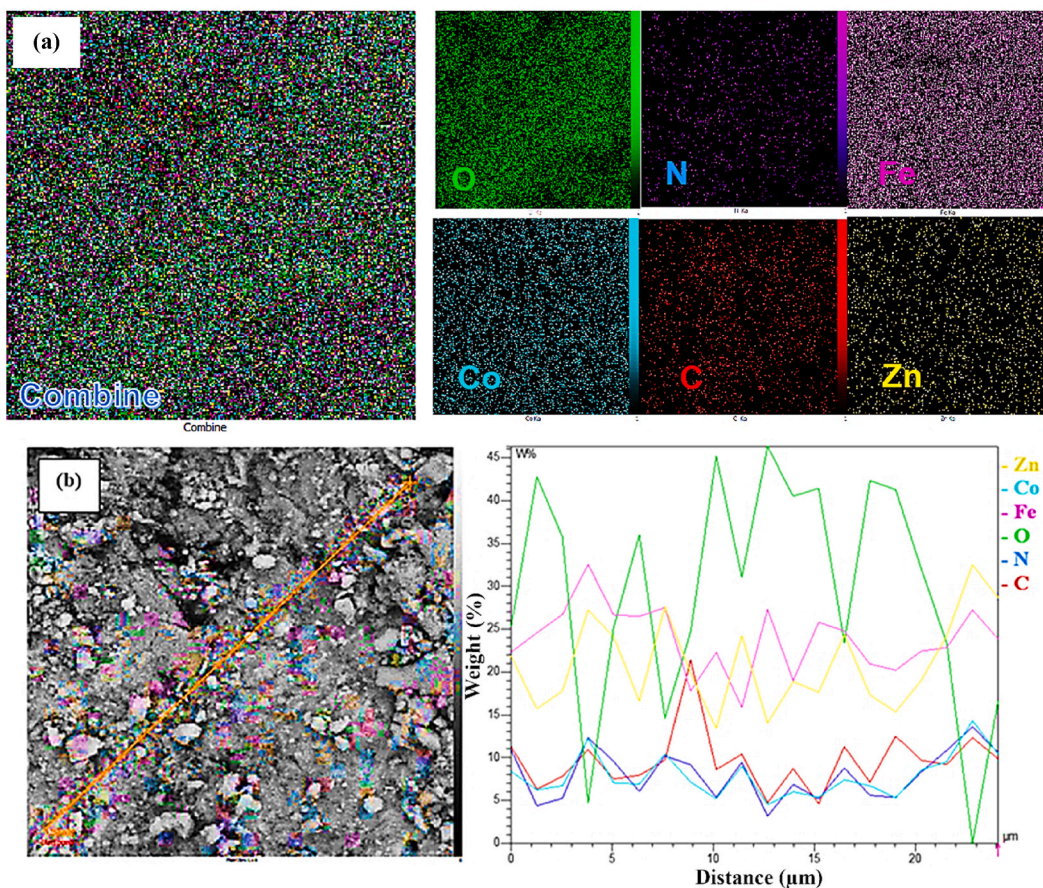
Fig. 4. Mapping (a) and line scanning (b) of ZnCoFe$_2$O$_4$@Ch magnetic nanoadsorbent.
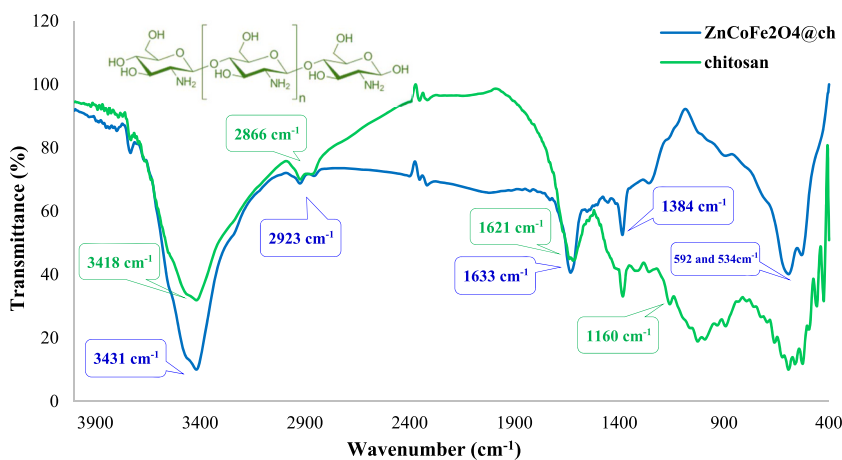
Fig. 5. FTIR spectra of ZnCoFe$_2$O$_4$@Ch magnetic nanoadsorbent and Chitosan.

nanosorbents were as follows:

Stretching vibrations of the O–H group were found in the range of 3431 cm^{-1}, stretching vibrations of the methylene –CH$_2$ group in the range of 2923 cm^{-1}, bending vibrations of the NH$_2$ amine group in the range of 1633 cm^{-1}, and C–N stretching vibrations in the range of 1384 cm^{-1} [62,65]. Additionally, the ferrite spinel ZnCoFe$_2$O$_4$@Ch has two absorption bands in the range of 592 and 534 cm^{-1} that are related to metal oxides in the octahedral and quadrilateral structures, respectively [66,67]. These findings support the effective synthesis of the nano sorbent ZnCoFe$_2$O$_4$@Ch in the presence of chitosan.

The XRD patterns of Chitosan, ZnCoFe$_2$O$_4$, and ZnCoFe$_2$O$_4$@Ch magnetic nano-adsorbent are shown in Fig. 6a-c. XRD analysis was used to characterize structures, phases, and crystalline composition of ZnCoFe$_2$O$_4$@Ch. The achieved results are shown in Fig. 6. The XRD pattern of Chitosan presents a prominent peak centered at 19.67°. Based on the JCPDS 96-591-0064, the ZnCoFe$_2$O$_4$@Ch crystal phase structure and XRD pattern with diffraction peaks at 2θ = 35.47°, 43.12°, 57.37°, 62.87° and 67.87° are indexed to the ZnCo-Fe$_2$O$_4$ cubic spinel phase. According to the obtained results, the ZnCoFe$_2$O$_4$ crystal structure was well-formed. It is so interesting that the XRD spectrum of ZnCoFe$_2$O$_4$@Ch indicates the characteristic peaks linked with chitosan and ZnCoFe$_2$O$_4$, which points to the successful synthesis of ZnCoFe$_2$O$_4$@Ch magnetic nanoadsorbent [59–61].

Fig. 7 shows adsorption/desorption isotherm, BET-BJH specific surface area, and t-plot of the synthesized ZnCoFe$_2$O$_4$@Ch (Fig. 7a–d). According to the BET plot the specific surface area, mean pore diameter, and total pore volume of synthesized magnetic nano adsorbent were obtained at 85.65 m^2/g, 6.86 nm, and 0.14 cm^3/g, respectively. ZnCoFe$_2$O$_4$@Ch could be classified as a mesoporous material [68]. Also, the high specific surface area of the nano-adsorbent (85.65 m^2/g) causes more interaction with the TC as a pollutant, which will increase the removal efficiency of the process. The literature also confirms these results [59–61].

By using a vibrating sample magnetometer, the magnetic properties of ZnCoFe$_2$O$_4$@Ch magnetic nano adsorbent were examined (Fig. 8a). The remnant magnetization (Mr), saturation magnetization (Ms), and coercive force (Hc) values were obtained 6.29 emu/g, 48.03 emu/g, and 50 Oe, respectively. These values depict the high magnetic strength of ZnCoFe$_2$O$_4$@Ch magnetic nano adsorbent. The results demonstrate that the ZnCoFe$_2$O$_4$ magnetic property in the ZnCoFe$_2$O$_4$@Ch structure is completely preserved.

TGA analysis was carried out to evaluate the thermal stability of ZnCoFe$_2$O$_4$@Ch in the temperature range 25 °C–800 °C, and results are depicted in Fig. 8b. The first mass loss step happened in the temperature range of 25 °C up to about 200 °C which is linked with the adsorbed water loss (−1.46 %). Due to the breakdown of Ch glycosidic bonds and also, its decomposition into lower fatty acids, the weight loss was reported at 200–800 °C (−3.82 %). According to the results, the adsorbent total weight loss was seen as 5.28 % until 800 °C which shows the ZnCoFe$_2$O$_4$@Ch high thermal stability. The TGA results of this research were confirmed by previous research that used nanocomposites of chitosan as adsorbents [59–61].
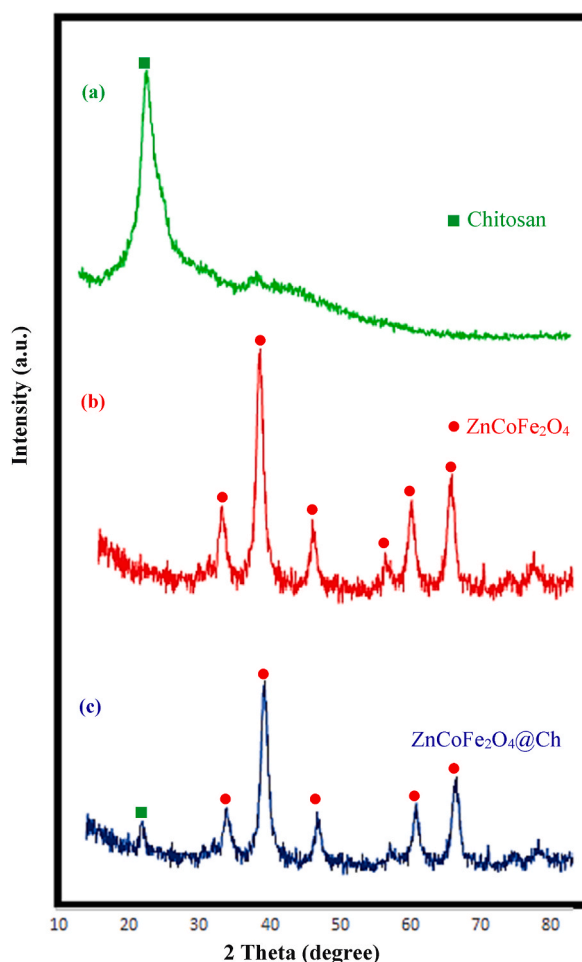
Fig. 6. The XRD patterns of Chitosan (a), ZnCoFe$_2$O$_4$ (b), and ZnCoFe$_2$O$_4$@Ch (c) magnetic nanoadsorbent.
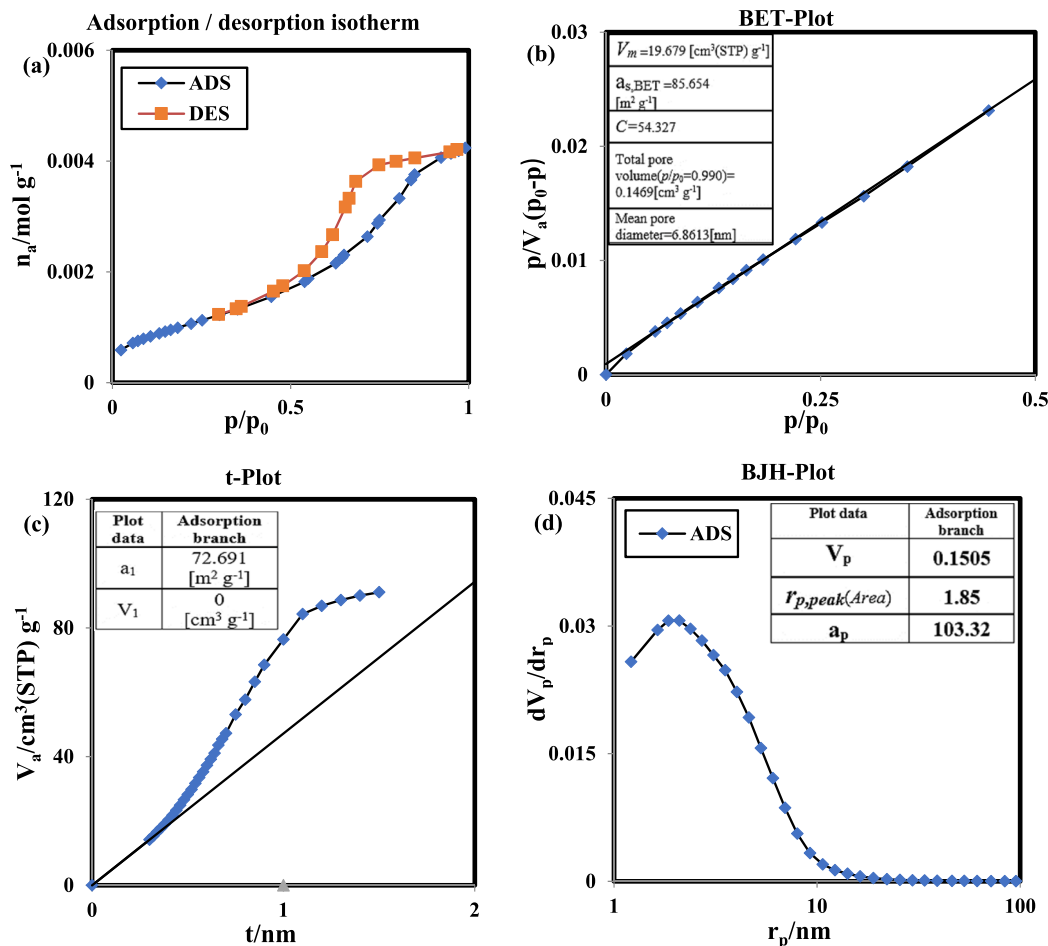
Fig. 7. Adsorption/desorption isotherm (a), BET surface area (b), t-Plot (c), and BJH surface area (d) of ZnCoFe$_2$O$_4$@Ch magnetic nanoadsorbent.

3.2. Adsorption test optimization

3.2.1. Effect of adsorbent dose

Fig. 9 (a) illustrates the impact of the nanosorbent's quantity on the effectiveness of TC removal after 45 min. The initial TC concentration in this method was 10 mg/L, the initial solution volume was 100 mL, and several doses of nanosorbents (0.7, 1, 1.5, and 2 g/L) were examined. The adsorption efficiency of TC was enhanced from 77 % to 85 % by increasing the quantity of nano sorbent from 0.7 to 1 g/L. The removal effectiveness improved by 93 % at higher nano sorbent doses of 2 g/L, but because this rise in removal efficiency was not evident and was not cost-effective, the optimal dose of 1 g/L nano sorbent with 85 % removal efficiency was taken into consideration. The increased contact area of the adsorbent and the availability of additional adsorption sites might have contributed to an increase in removal effectiveness with increasing adsorbent dosage. On the other hand, since the concentration of TC was constant and the amount of interaction between the antibiotic molecules and the adsorbent nanoparticles did not greatly rise, its adsorption rate did not dramatically increase with increasing adsorbent dosage. In the process of removing TC using magnetic nanosorbents (Fe-MCM-41-A), Guo et al. observed that by increasing the dose from 0.1 g/L to 1 g/L 1, the removal efficiency increased from 47 % to 98 %. This observation is consistent with the findings of this study and can be attributed to the increase in the level of adsorbent contact [69].

3.2.2. Effect of pH

In the adsorption process, the impact of pH is substantial. Under the premise that the initial concentration of TC was 10 mg/L and the ideal quantity of nano sorbent (1 g/L), the results of the influence of pH on the removal effectiveness of TC by magnetic nano-composite are demonstrated in a period of 2–45 min (Fig. 9b). As the pH was 3, the maximum removal effectiveness was 85 %, and when the pH rose to 11, it fell to 9 %. As a result, 3 was considered to be the optimum pH. On the other hand, the adsorbent pH$_{zpc}$ also has an impact on the effectiveness of the adsorption process. Similar to this, the pH$_{zpc}$ of ZnCoFe$_2$O$_4$@Ch nano sorbent was measured, and its value was reported to be 6.8 (Fig. 9d). According to the pH$_{zpc}$ value for the nano sorbent, it was revealed that the adsorbent
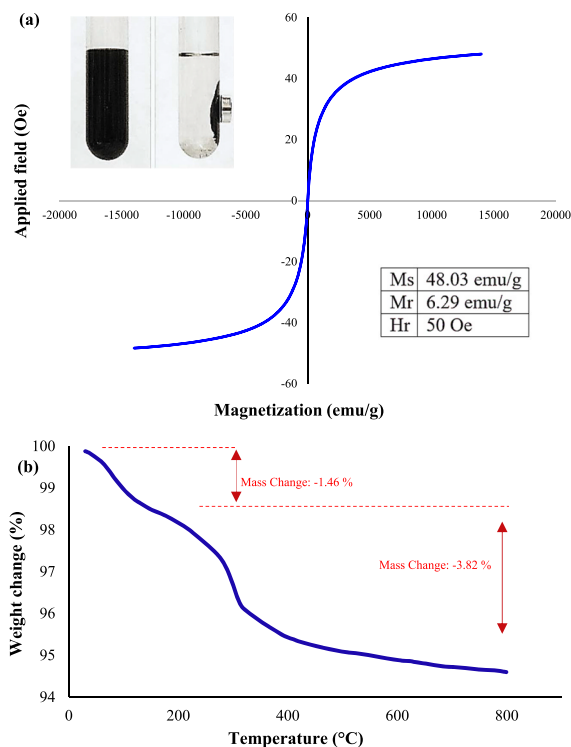
Fig. 8. VSM magnetization curve of ZnCoFe$_2$O$_4$@Ch magnetic nano adsorbent; the photo inset shows the solution after magnetic separation of the magnetic nano adsorbent and (a) the TGA pattern of ZnCoFe$_2$O$_4$@Ch (b).

surface is positive at pHs below 6.8 and negative at pHs over 6.8. Given that TC has three acid dissociation constants (pKa) of 3.3, 7.68, and 9.68, as shown in Fig. 9c, it can exist in a variety of ionic forms at various pH levels. Between pH 3.3 to 7.68, TC molecules may be found in zwitterion or neutral form, at pH 3.3 can be found in cationic form, and above pH 7.68, they can be found in the anionic form [70]. Since the optimum pH for this method is claimed to be 3, the presence of the tetracycline molecule in cationic form and the positive charge on the adsorbent surface means that electrostatic attraction forces won't be a major factor in the adsorption of pollutants on the adsorbent surface at this pH. Therefore, TC tends to separate from the aqueous medium under the influence of lyophobic forces and reach the surface of the adsorbent under these circumstances because it is an organic compound in the aqueous medium. As a result, this mechanism in the adsorption of TC on the adsorbent was predominant [71]. Luo et al.'s study on the adsorption of TC through modified alginate grains revealed that a pH of 5 was ideal for the process. Thus, compared to neutral and alkaline pHs, acidic pHs had the best effectiveness, which is consistent with the findings of this study [72].

3.2.3. Effect of the initial concentration

Tetracycline solutions at concentrations of 5, 10, 15, 20, and 30 mg/L, with an optimum pH of 3, and a temperature of 25 °C were in contact with 1 g/L of ZnCoFe$_2$O$_4$@Ch magnetic nano sorbent to examine the impact of variations in TC concentration on its removal effectiveness (Fig. 9e). According to the findings of concentration changes, the adsorption effectiveness of TC declined from 90 % to 67 % when the initial concentration of TC solution was increased from 5 mg/L to 30 mg/L. As a consequence, the ideal concentration of TC in the process was 5 mg/L. Since the solution's TC molecule density rises with the initial concentration, the active sites on the adsorbent surface are occupied more quickly, and the effectiveness of TC removal declines [73]. According to Kasraei et al.'s work on the removal of TC from wastewater using the adsorption process (Fe$_3$O$_4$@TOMATS IL), the removal efficiency fell as the concentration of TC rose, which is consistent with the findings of this investigation [74].

3.2.4. Effect of temperature

Another factor influencing the adsorption process is the temperature. Fig. 9 (f) depicts the influence of temperature fluctuations on the adsorption efficiency of tetracycline. At a concentration of 5 mg/L of TC and pH 3, the findings of the investigation on the influence of process temperature (25, 35, 45, and 55 °C) on the removal efficiency of TC by magnetic nano sorbent revealed that at 25 °C temperature, 90 % of the antibiotic was effectively adsorbable. Tetracycline's removal effectiveness dropped to 86 % at 55 °C due to a reduction in removal rate as the temperature rose to that point. This outcome demonstrates the exothermic nature of the adsorption process as well as physical adsorption. Because raising the temperature did not improve efficiency, chemical adsorption did not take place; instead, physical adsorption occurred. van der Waals forces had a stronger impact on physical adsorption, which increased the adsorption efficiency [7]. The trend of negative ΔH values in Ahmad et al.'s research for the removal of TC by poly
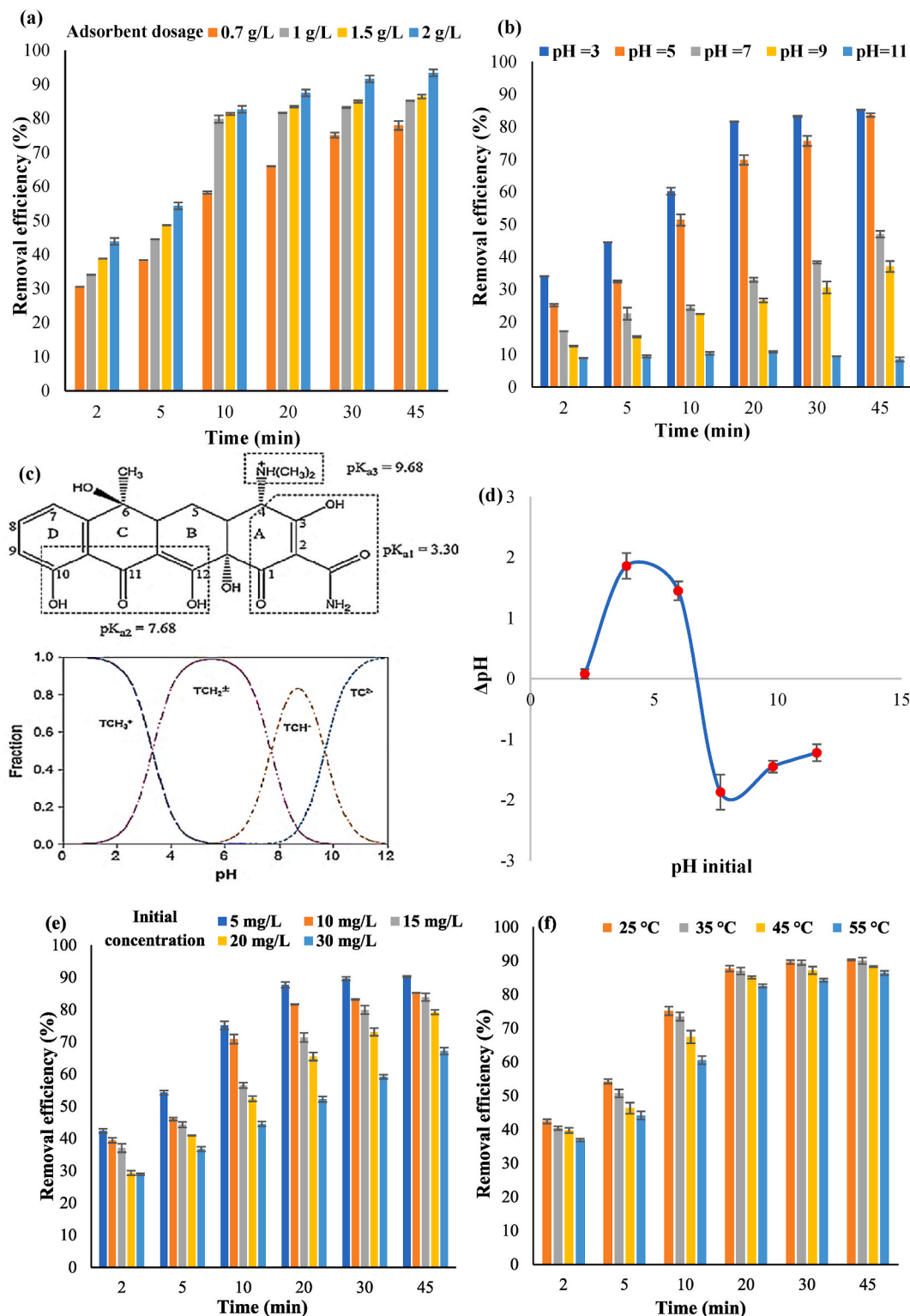
Fig. 9. Effect of adsorbent dose (a), pH (b), the ionic forms of TC at different pHs (c), pH$_{zpc}$ (d), TC concentration (e), and temperature (f) (optimum condition: pH: 3, nanoadsorbent dosage: 1 g/L, TC initial concentration: 5 mg/L, and temperature: 25 °C).

(cyclotriphosphazene-*co*-4,4′-sulfonyldiphenol)/rGO suggested that the adsorption process was exothermic, which is compatible with the results of the current study [75].

3.3. Adsorption isotherm models

In this process, the equilibrium state of the adsorbate on the adsorbent surface was studied using the Langmuir and Freundlich isotherms. According to the Langmuir model (Eq. (3)), adsorption occurs as a single layer, with the adsorbate molecule on the adsorbent surface and constant adsorption energy. The adsorption of one molecule at a site does not impact the adsorption of other molecules at the same site [76].

$$\frac{C_e}{Q_e} = \frac{1}{Q_{max}K_L} + \frac{C_e}{Q_{max}}$$ (Eq. 3)

The maximum adsorption capacity is represented in this equation by Q_{max} (mg/g). The equilibrium concentration of TC is expressed as C_e (mg/L), the quantity of the adsorbed substance is expressed as Q_e (mg/g), and Langmuir's adsorption equilibrium constant is expressed as K_L (L/mg).

R_L (Eq. (4)), which studies the state of the adsorption process, is another parameter. Thus, the adsorption process is irreversible if $R_L = 0$, the favorable adsorption process if $1 > R_L > 0$, the linear adsorption process if $R_L = 1$, and the unfavorable adsorption process if $R_L > 1$ [77].

$$R_L = \frac{1}{1 + K_L\,C_0}$$ (Eq. 4)

where tetracycline's initial concentration in mg/L is represented by C_0 in this equation.

The Freundlich model (Eq. (5)) may be utilized for heterogeneous surface adsorption as well as multilayer adsorption with heterogeneous heat distribution.

$$\log q_e = \log K_F + \frac{1}{n}\,\log C_e$$ (Eq. 5)

Freundlich's adsorption equilibrium constant is K_F ((mg/g) (L/mg)$^{1/n}$) in this equation. The kind of isotherm is indicated by the heterogeneity factor, also known as surface adsorption intensity or $1/n$. In other words, the adsorption process is reversible if $1/n = 0$, favorable if $0 > 1/n > 1$, and unfavorable if $1 > 1/n$ [78]. Fig. 10 (a, b) shows the findings from studied Langmuir and Freundlich equilibrium isotherms.

The contacts between the adsorbent and the adsorbate are taken into consideration by the Temkin isotherm. Under Temkin isotherm, the temperature of adsorption in several layers declines logarithmically as a result of the reciprocal impacts of the adsorbent and the adsorbate on one another. Equations (6) and (7) display the Temkin isotherm's linear formula.

$$Q_e = BTlnK_t + BTlnC_e$$ (Eq. 6)

$$bT = (RT)\,/\,(BT)$$ (Eq. 7)

As BT and bT are constants in these equations, K_t stands for the Temkin adsorption potential (L/g). T is the absolute temperature in Kelvin, and R is the universal gas constant (8.314 J/mol.K).

To consider the impact of the porous structure of adsorbents, the Dubinin-Radushkevich isotherm model is utilized. It clarifies the porosity and adsorption energy of the adsorbent. The linear formula for the Dubinin-Radushkevich isotherm is shown in equations (8) and (9) [1,3].

$$\ln q_e = \ln q_m - \beta \cdot \varepsilon^2$$ (Eq. 8)
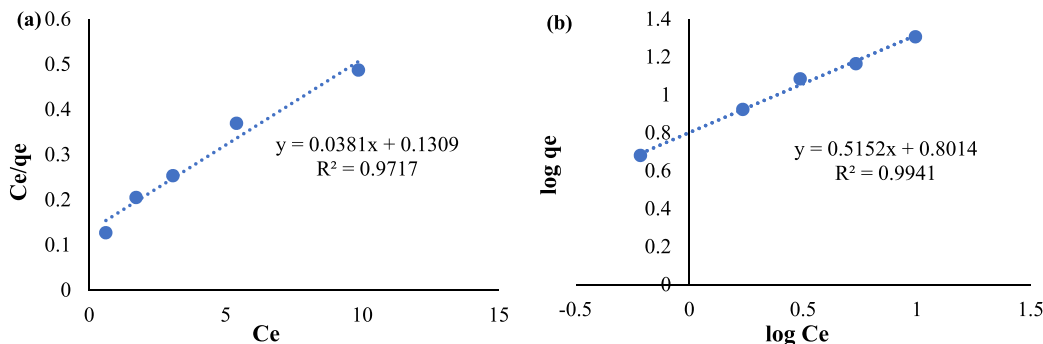
Fig. 10. Langmuir (a) and Freundlich (b) isotherm plot (adsorbent: 1 g/L, contact time: 30 min, pH: 3, and temperature: 25 °C).

$$\varepsilon = RTln\left(\frac{C_0}{C_e}\right) \tag{Eq. 9}$$

The adsorption energy is represented by the constant β (mol^2/kJ^2), while the adsorption potential is represented by ε (kJ/mol). Table 1 displays the results from studied Freundlich, Langmuir, Temkin, and Dubinin-Radushkevich equilibrium isotherms.

The findings shown in Table 1 imply that the Freundlich model's R^2 value (R^2 = 0.994) was higher than the Langmuir model's R^2 value (R^2 = 0.972). The Freundlich isotherm model is, therefore, more fitted to describe the adsorption process. Additionally, the Freundlich model's value of *1/n* lies between 0 and 1, suggesting that adsorption is preferable. The results of this work are compatible with Luo et al.'s isotherm study for the adsorption of TC from aqueous solutions by modified alginate beads, which demonstrated that the adsorption process of TC follows the Freundlich isotherm [72].

3.4. Kinetic study

To comprehend the dynamics and the impact of variables impacting the rate of tetracycline adsorption on the adsorbent, adsorption kinetics was studied. In this investigation, model kinetics of *pseudo*-first-order (Eq. (10)), *pseudo*-second-order (Eq. (11)), and intra-particle kinetic model (Eq. (12)) were employed.

$$\ln(q_e - q_t) = \ln q_e - K_1 t \tag{Eq. 10}$$

The *pseudo*-first-order model's speed constant is K_1 (min^{-1}) in this equation. Tetracycline adsorbed amounts are shown in q_e (mg/g) and q_t (mg/g), respectively, for the equilibrium state and given periods (min).

$$\frac{t}{q_t} = \frac{1}{K_2 q_e^2} + \frac{1}{q_e} \times t \tag{Eq. 11}$$

where K_2 (g/mg. min) is the *pseudo*-second-order kinetic constant in this equation. Tetracycline adsorbed amounts are shown in q_e and q_t (mg/g), respectively, at equilibrium and at any given time (min). The slope of the linear graph of the equation may be used to determine the speed constant K_2 [79]. Fig. 11 (a, b) shows the findings from the studied *pseudo*-first-order and *pseudo*-second-order kinetic models.

The restricting phase that regulates the kinetics in the majority of adsorption processes is frequently thought of as intraparticle diffusion kinetics. The quantity of absorbance against the square of time, as represented by Weber and Morris, is plotted to determine the likelihood of kinetic limiting by transport in pores [80].

$$q_t = K_i t^{0.5} + C \tag{Eq. 12}$$

where K_i (g/mg.min) in this correlation stands for the particle's internal diffusion rate constant and C for the boundary layer's penetration or surface adsorption.

The Elovich equation is appropriate for systems with heterogeneous adsorbing surfaces and can be met by chemical adsorption processes, which describe many pollutant adsorption systems. The following equation (Eq. 13) serves as a foundation for calculating this kinetic model.

$$q_t = 1/\beta \ln (\alpha \cdot \beta) + 1/\beta \ln t \tag{Eq. 13}$$

The initial adsorption rate constant in this equation is α (mg/g.min), while the desorption rate constant is β (g/mg) [81].

Table 2 reports the findings of the kinetic studies of the TC adsorption process by ZnCoFe$_2$O$_4$@Ch.

The *pseudo*-second-order model is used to describe the adsorption behavior since the value of R^2 in the *pseudo*-second-order kinetic model (R^2 = 0.996) is greater than the value of R^2 in the pseudo-first-order model (R^2 = 0.467). Therefore, TC adsorbed effectively on magnetic nano-adsorbent ZnCoFe$_2$O$_4$@Ch using a *pseudo*-second-order kinetic model. In agreement with the findings of this investigation, Zhang et al.'s kinetic assessment for the adsorption of TC using CoFe$_2$O$_4$/MMT magnetic nano-adsorbent revealed that the kinetics of the adsorption process followed *pseudo*-second-order kinetics [82].

Table 1

Langmuir, Freundlich, Temkin, and Dubinin-Radushkevich isotherm parameters (adsorbent: 1 g/L, contact time: 30 min, pH: 3, and temperature: 25 °C).

Langmuir				Freundlich			Temkin			Dubinin-Radushkevich		
R^2	R$_L$	Q$_{max}$ (mg/g)	K$_L$	R^2	K$_F$	1/n	R^2	B$_1$	K$_T$ (L/mg)	Q$_{max}$ (mg/g)	E (kJ/mol)	R^2
0.972	0.408	26.241	0.291	0.994	6.321	0.515	0.963	5.419	3.289	7.295	31.623	0.827
	0.256											
	0.187											
	0.147											
	0.103											

Fig. 11. *Pseudo*-first-order (a) and *pseudo*-second-order (b) kinetic plot (TC: 5 mg/L, Adsorbent: 1 g/L, pH: 3, and temperature: 25 °C).

Table 2
Coefficients for the adsorption kinetics models (TC: 5 mg/L, adsorbent: 1 g/L, pH: 3, and temperature: 25 °C).

Pseudo-first-order kinetic model			*Pseudo*-second-order kinetic model			Intraparticle kinetic model			Elovich kinetic model		
R^2	K_1 (1/min)	q_e (mg/g)	R^2	K_2 (g/mg.min)	q_e (mg/g)	R^2	K_P (mg/g. min^{-5})	C (mg/g)	R^2	β (g/mg)	α (mg/g.min)
0.467	0.040	1.930	0.996	0.057	5.661	0.975	0.594	2.108	0.991	1.088	8.516

3.5. Thermodynamic study

Thermodynamic characteristics, such as variations in Gibbs free energy (ΔG), enthalpy (ΔH), and entropy (ΔS), may be studied using variations in the equilibrium constant with temperature in the equilibrium state. Equation (14) was used to determine how the adsorption process's Gibbs free energy fluctuates.

$$\Delta G = -RTln \; k_d \quad \text{(Eq. 14)}$$

in this equation, ΔG is the Gibbs free energy change (KJ/mol), R is the general constant of gases (J/mol. K), and T is the temperature (K). Equation (15) was also used to find the equilibrium constant (K_d).

$$K_d = \frac{(C0 - Ce)}{Ce} \times \frac{V}{W} \quad \text{(Eq. 15)}$$

in this equation, the initial and equilibrium concentrations are C_0 (mg/L) and C_e (mg/L), respectively, as well the volume of the solution is V (L) and the mass of the adsorbent is W (g). The values of the standard enthalpy changes (ΔH) and standard entropy changes (ΔS) can be obtained by drawing the *Van't Hoff* plot, which is lnK_d versus $1/T$ (Fig. 12), and then determining the equation of the line and gain enthalpy and entropy changes values (Eq. (16)) [77].

$$ln \; K_d = \frac{\Delta s}{R} - \frac{\Delta H}{RT} \quad \text{(Eq. 16)}$$

Table 3 summarizes the findings of thermodynamic studies of the TC adsorption process on the ZnCoFe$_2$O$_4$@Ch.

The findings are compatible with Yu et al.'s study on the adsorption of TC antibiotic through magnetic graphene oxide, where the negative Gibbs free energy of the process shows that the adsorption process is carried out spontaneously [83]. The exothermic character of the adsorption process is shown by the negative of the typical enthalpy changes. Additionally, the negative standard
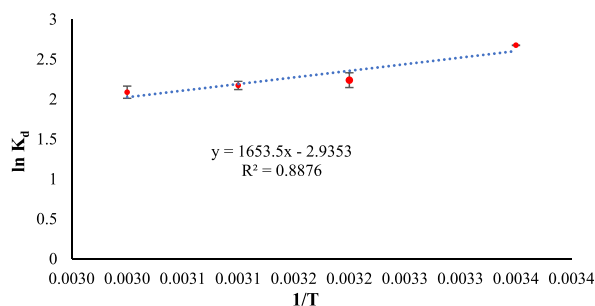
Fig. 12. *Van't Hoff* plot (pH: 3, nano adsorbent dosage: 1 g/L, TC initial concentration: 5 mg/L).

Table 3

Thermodynamic parameters of TC adsorption onto ZnCoFe$_2$O$_4$@Ch (pH: 3, nanoadsorbent dosage: 1 g/L, TC initial concentration: 5 mg/L).

T (k)	ΔG (kJ/mol)	ΔH (kJ/mol)	Δ**S** (j/mol.k)
298	−6.621	−15.162	−28.694
308	−5.730		
318	−5.742		
328	−5.693		

entropy changes show less disorder in the adsorption process. These findings are in accordance with the research by Turku et al. on the adsorption of TC by silica, which used typical enthalpy and entropy changes [84].

3.6. Investigation of process efficiency on real wastewater

Tetracycline adsorption was also evaluated on a real wastewater sample from Kerman University of Medical Sciences under ideal circumstances (pH: 3, nano adsorbent dosage: 1 g/L, contact time: 30 min, temperature: 25 °C). Table 4 reports the findings of the physio-chemical quality of this effluent.

The real sample's maximum adsorption efficiency was attained at a rate of 80 %. The presence of interfering elements in the wastewater sample, such as anions and cations, prevents the adsorption of the TC pollutant on the adsorbent surface and competes with TC for adsorption on the adsorbent surface, resulting in a drop in efficiency in the real sample. The results of this study were similar to Nasiri et al.'s study [7].

3.7. Comparison of the ZnCoFe$_2$O$_4$@Ch performance with other adsorbents

In Table 5, the effectiveness of magnetic nanocomposite ZnCoFe$_2$O$_4$@Ch in removing medicinal substances was contrasted with that of other synthetic magnetic adsorbents. ZnCoFe$_2$O$_4$@Ch magnetic nanocomposite had greater removal effectiveness in less time and adsorbent dosage, as well as higher adsorption capacity, according to Table 5.

3.8. Chemical stability and reusability of ZnCoFe$_2$O$_4$@Ch

Recovery and reusing of the adsorbent are crucial to the adsorption process from an economic and environmental perspective. Due to its strong magnetic properties, the magnetic nanocomposite ZnCoFe$_2$O$_4$@Ch is easily separated from the process environment by a magnet and does not cause secondary environmental contamination. After separating the adsorbent from the process medium using a magnet, it was put in a furnace at 200 °C for 1 h to remove the pollutants adsorbed on the adsorbent in order to assess the reusability of the employed nano sorbent. Then, under ideal circumstances, five recovery cycles were used to evaluate its effectiveness [69]. The removal effectiveness of the magnetic nanocomposite ZnCoFe$_2$O$_4$@Ch fell from 93 % to 89 % during two cycles. As shown in Fig. 13a, the removal effectiveness was 65 % after five recovery cycles (TC: 5 mg/L, Adsorbent: 1 g/L). After five stages of usage and regeneration, the ANOVA analysis revealed that there is no significant difference (p = 0.201) between the various cycles of adsorbent regeneration, indicating the satisfactory functioning of the adsorbent. The pollutant's presence in adsorbent sites may be the cause of this drop in efficiency, so, the explanation for the decline in TC removal effectiveness after five cycles of recovery and reuse may be attributed to the irreversible occupancy of the active sites of the adsorbent. According to Weng et al.'s study, after three cycles of using magnetic nanosorbents to remove the antibiotics ofloxacin and pefloxacin, antibiotic adsorption was 50 % and 67 % efficient, respectively (76). By using XRD, FESEM, and VSM analysis, the chemical stability of the adsorbent after five cycles of reuse and recovery was evaluated (Fig. 13b, c, and d). According to the XRD, FESEM, and VSM analysis, the nano adsorbent's crystal structure, morphology, and magnetic strength are still retained after five steps of recovery and may be utilized again to treat wastewater that contains TC. Also, the morphological properties of the adsorbent were still present after the fifth cycle, per the FESEM findings. There

Table 4

Physicochemical characteristics of real wastewater samples.

Parameter	Value
pH	7.35
SO$_4$ (mg/L)	134.5
BOD$_5$ (mg/L)	8
COD (mg/L)	26.1
TSS (mg/L)	78
TDS (mg/L)	1194
N (NH3) (mg/L)	1.4
TKN (mg/L)	1.82
PO$_4$ orto (mg/L)	38.38
Tetracycline (mg/L)	5

Table 5
Comparison of ZnCoFe$_2$O$_4$@Ch with other adsorbents.

No.	Adsorbent	Pollutant	Dose of adsorbent (g/L)	Concentration (mg/L)	Contact time (min)	Efficiency (%)		Recovery (%) \	Adsorption capacity	Ref.
						Synthetic sample	Real sample \			
1	Biochar (Rice straw)	Tetracycline	3	32.5	1440	92	–	–	13	[85]
2	Magnetic GAC	Metronidazole	1	20	90	92	–	–	–	[86]
3	AC-Fe$_3$O$_4$	Amoxicillin	1	50	90	90	–	–	–	[87]
4	Biochar rice	Tetracycline	1.5	10	60	70	–	–	13.33	[88]
5	Biochar rice	Metronidazole	1.5	10	45	90	–	–	21.33	[88]
6	Magnetic iron nanoparticles (nFe)	Ofloxacin	0.2	5	300	100	56	67	12.8	[89]
7	ZnCoFe$_2$O$_4$@Ch	Tetracycline	1	5	30	93	80	65	26.24	This work
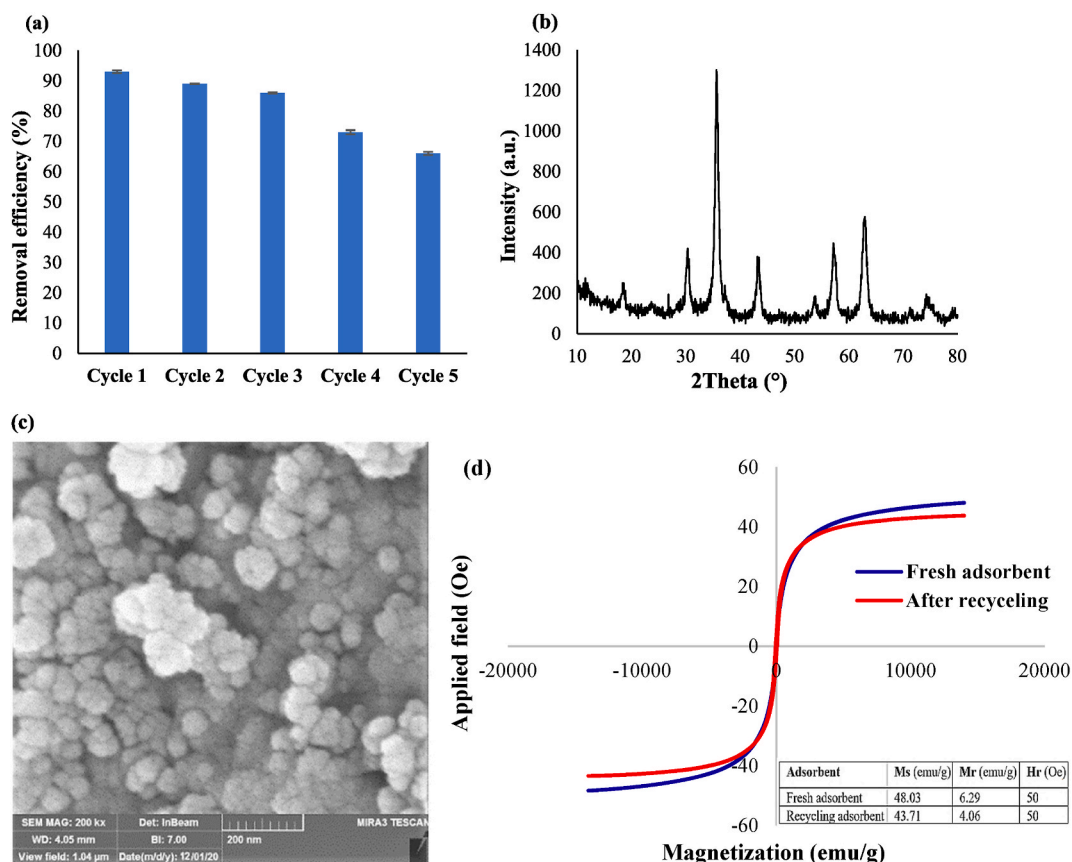
Fig. 13. Recycling of ZnCoFe$_2$O$_4$@Ch in the removal of TC (pH: 3, nano adsorbent dosage: 1 g/L, TC initial concentration: 5 mg/L) (a), XRD (b), FESEM (c) and VSM (d) analysis after five recovery steps.

was no discernible change in the location of 2 Theta in the XRD analysis pattern. Additionally, the XRD analysis's strong peaks show the adsorbent's great chemical stability.

3.9. Adsorption mechanism

The FTIR spectrum of the adsorbent before and after the adsorption process has been investigated to better understand how TC is adsorbed into the adsorbent surface (Fig. 14a). Following the adsorption process, the strength of several peaks has changed in the absorber's FTIR spectrum, shifting to a lower wavelength. This suggests that these groups took part in the TC adsorption process. It is clear from the spectra that the band around 3431 cm^{-1} corresponding to the stretching vibrations of the hydroxyl functional groups is shifted to a lower wavelength of 3410 cm^{-1}, the band around 2866 cm^{-1} corresponding to the stretching vibrations of the C–H group to a lower wavelength of 2848 cm^{-1}, the band around 1621 cm^{-1} corresponding to the bending vibrations of amine group to a lower wavelength of 1614 cm^{-1}, and two absorption bands in the range of 592 cm^{-1} and 534 cm^{-1}, associated to metal oxides in the octahedral and tetrahedral structure of ferrites spinel of nano adsorbent to lower wavelengths of 584 cm^{-1} and 467 cm^{-1}, respectively, and their intensities were reduced after TC adsorption, suggesting the participation of these groups in the TC adsorption process.

The mechanisms that may influence TC adsorption by ZnCoFe$_2$O$_4$@Ch nanosorbents are discussed further below. Through various forces acting on the TC and the adsorbent during the TC adsorption process, these interactions may take effect. Different regions of the ZnCoFe$_2$O$_4$@Ch nano sorbent can interact with the π electrons of the aromatic ring of the TC molecule. The π electrons of the TC aromatic ring can establish a CH- π bond with the CH groups in the chitosan structure [90,91]. Therefore, the van der Waals attraction force between the π electrons of the aromatic ring of the TC molecule and the hydrogen atom of the CH group in chitosan is necessary for the adsorption of TC molecules by the matrix structure of chitosan to generate a CH-π bond. The formation of an NH$_2$/OH-π bond with the amine group or the hydroxyl of chitosan is another hypothesis that may be involved in the TC adsorption process [91]. Chitosan is a polar compound that tends to produce hydrogen bonds with hydrophobic substances like TC since it has amine and hydroxyl groups in its structure [91,92]. The OH and NH$_2$ groups in the chitosan structure can form hydrogen bonds with the TC molecule's organic and hydrophobic nature. Additionally, in the adsorbent structure of ZnCoFe$_2$O$_4$@Ch, metal ions of transition metals including cobalt, zinc, and iron can function as either Lewis's acids or electron receptors. Functional groups in the TC structure like hydroxyl, amine, and carbonyl may also act as electron donor groups (EDGs) for transition metals such as cobalt, zinc, and iron.
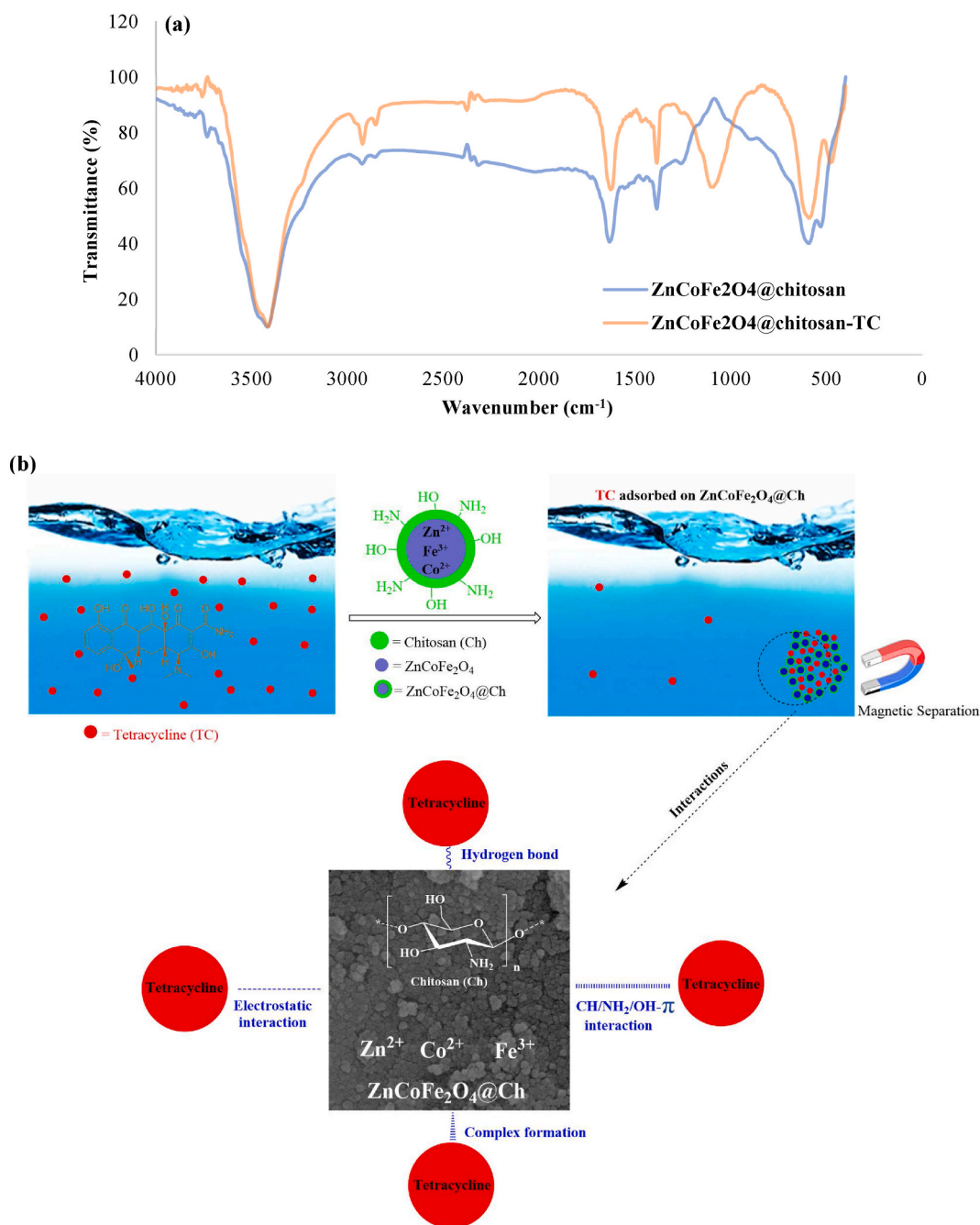
Fig. 14. FTIR of ZnCoFe$_2$O$_4$@Ch before and after Tetracycline adsorption (a) and proposed mechanisms for TC adsorption on the ZnCo-Fe$_2$O$_4$@Ch (b).

The EDGs of TC interact with the metal ions of the transition metals as electron-withdrawing groups (EWGs) to form a complex between the TC and the adsorbent. The development of this complex may have an impact on the process of TC adsorption [54,55]. Fig. 14b shows a schematic of the potential pathways for the ZnCoFe$_2$O$_4$@Ch nanocomposite's TC adsorption process.

3.10. The performance comparison of ZnCoFe$_2$O$_4$@Ch, ZnCoFe$_2$O$_4$, and Ch in TC removal

Fig. 15 compares the TC adsorption efficiencies of ZnCoFe$_2$O$_4$@Ch, ZnCoFe$_2$O$_4$, and Ch under optimum adsorption conditions. The results showed that ZnCoFe$_2$O$_4$@Ch, ZnCoFe$_2$O$_4$, and Ch were able to remove 93 %, 82 %, and 65 % of TC, respectively. Compared to ZnCoFe$_2$O$_4$@Ch and ZnCoFe$_2$O$_4$, chitosan was less effective in TC removal despite having functional groups. Also, the separation of Ch
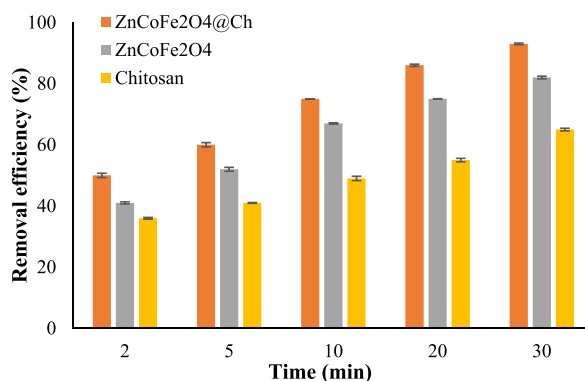
Fig. 15. The performance comparison of $ZnCoFe_2O_4@Ch$, $ZnCoFe_2O_4$, and Chitosan for TC adsorption (temperature = 25 °C, pH = 3, dosage nano-adsorbent = 1 g/L, concentration TC = 5 mg/L).

from the process solution should be done by filtration, which is very time-consuming. In addition, Ch is not in the nanoscale and has a smaller surface area compared to $ZnCoFe_2O_4@Ch$ and $ZnCoFe_2O_4$, and its adsorption capacity is lower. $ZnCoFe_2O_4$ nanoparticles compared to Ch were more effective in removing TC. However, their efficiency was lower than $ZnCoFe_2O_4@Ch$. $ZnCoFe_2O_4$ nanoparticles have a larger surface area compared to Ch because they are on a nanoscale, and due to their magnetic properties, they are easily and quickly separated from the process solution. But the efficiency of $ZnCoFe_2O_4$ nanoparticles was lower than the $ZnCoFe_2O_4@Ch$. Because the hydroxyl and amine functional groups present in the $ZnCoFe_2O_4@Ch$ structure help the TC adsorption process. Following the experiments, the significance level between the antibiotic adsorption efficiency with chitosan, $ZnCoFe_2O_4$, and $ZnCoFe_2O_4@Ch$ was analyzed by ANOVA using the software SPSS v. 21. It was discovered that there was a significant difference ($p < 0.046$) between the adsorption efficiency of these adsorbents.

4. Conclusion

In summary, $ZnCoFe_2O_4@Ch$ as a recyclable and environmentally friendly magnetic nanohybrid adsorbent was prepared with the microwave-assisted co-precipitation method. The structural characteristics of the produced $ZnCoFe_2O_4@Ch$ were investigated by using various analyses. The nano-scale adsorbent was synthesized as homogenous, lump-free, quasi-spherical nanoparticles with large surface areas and magnetic properties while preserving the crystalline structure. Tetracycline was removed from synthetic and real wastewater samples by $ZnCoFe_2O_4@Ch$ in 93 % and 80 %, respectively, under optimal conditions. Tetracycline adsorption is confirmed by adsorption kinetics and isotherms to be compatible with *pseudo*-second-order kinetic and the Freundlich isotherm, respectively. The adsorption process is exothermic, accompanied by the reduction of entropy and spontaneously, according to the findings of the analysis of thermodynamic data. After five cycles of reuse and recovery, the synthesized magnetic nanocomposite was able to remove 65 % of TC from the aqueous environment. Tetracycline may be eliminated from contaminated water and wastewater from the pharmaceutical industries using this magnetic nanocomposite. The findings of the study showed that various polysaccharides, including methylcellulose, carboxymethyl cellulose, and starch, may one day be utilized to change various magnetic nano adsorbents and be incorporated into the development of useful magnetic nanocomposites. These polysaccharides may be utilized to modify ferritic metal spinels, which can then be employed as heterogeneous magnetic nanocatalysts or magnetic nano adsorbents to remove diverse organic and inorganic contaminants from contaminated water environments. Also, the limitation statements include the following things that need more research in this field.

- The operating parameters of the batch adsorption, could handle a larger volume of wastewater?
- Would the operating parameters be feasible for real applications?
- Could the adsorbent effectively remove the pollutants if the concentration range differs?
- Is doing this process economically justified?

Data availability statement

Data will be made available on request.

Declaration of interest's statement

The authors declare that they have no known competing financial interests or personal relationships that could have appeared to influence the work reported in this paper.

Additional information

No additional information is available for this paper.

Approval of the submitted version of the manuscript

Please check this box to confirm that all co-authors have read and approved the version of the manuscript that is submitted. Signatures are not required.

CRediT authorship contribution statement

Alireza Nasiri: Writing – review & editing, Visualization, Validation, Supervision, Methodology, Investigation, Formal analysis, Conceptualization. **Najmeh Golestani:** Writing – original draft, Validation, Software, Methodology, Data curation. **Saeed Rajabi:** Writing – review & editing, Formal analysis, Data curation. **Majid Hashemi:** Writing – review & editing, Visualization, Validation, Supervision, Resources, Project administration, Methodology, Investigation, Funding acquisition, Formal analysis.

Declaration of competing interest

The authors declare that they have no known competing financial interests or personal relationships that could have appeared to influence the work reported in this paper.

Acknowledgments

References

[1] F. Hashemzadeh, S.H. Derakhshandeh, M.M. Soori, F. Khedri, S. Rajabi, Bisphenol A adsorption using modified aloe vera leaf-wastes derived bio-sorbents from aqueous solution: kinetic, isotherm, and thermodynamic studies, Int. J. Environ. Health Res. (2023) 1–21, https://doi.org/10.1080/09603123.2023.2208536.

[2] M. Iqhrammullah, S. Saleha, F.P. Maulina, R. Idroes, Polyurethane film prepared from ball-milled algal polyol particle and activated carbon filler for NH3–N removal, Heliyon 6 (8) (2020) e04590.

[3] S. Maleky, A. Asadipour, A. Nasiri, R. Luque, M. Faraji, Tetracycline adsorption from aqueous media by magnetically separable Fe3O4@ Methylcellulose/ APTMS: isotherm, kinetic and thermodynamic studies, J. Polym. Environ. 30 (8) (2022) 3351–3367.

[4] R. Morovati, S. Rajabi, M.T. Ghaneian, M. Dehghani, Efficiency of Ag3PO4/TiO2 as a heterogeneous catalyst under solar and visible light for humic acid removal from aqueous solution, Heliyon 9 (5) (2023) e15678, https://doi.org/10.1016/j.heliyon.2023.e15678.

[5] M.T.G. Roya Morovati, Saeed Rajabi, Mansooreh Dehghani, Degradation efficiency of humic acid in presence of hydrogen peroxide and ultrasonic from aqueous media, Desalination Water Treat. 281 (2023) 249–254.

[6] Z. Derakhshan, M. Mokhtari, F. Babaei, R. Malek Ahmadi, M.H. Ehrampoush, M. Faramarzian, Removal methods of antibiotic compounds from aqueous environments– A review, ssu-jehsd 1 (1) (2016) 43–62.

[7] A. Nasiri, S. Rajabi, A. Amiri, M. Fattahizade, O. Hasani, A. Lalehzari, M. Hashemi, Adsorption of tetracycline using CuCoFe2O4@ Chitosan as a new and green magnetic nanohybrid adsorbent from aqueous solutions: isotherm, kinetic and thermodynamic study, Arab. J. Chem. 15 (8) (2022) 104014.

[8] G.M. Eliopoulos, G.M. Eliopoulos, M.C. Roberts, Tetracycline therapy: update, Clin. Infect. Dis. 36 (4) (2003) 462–467, https://doi.org/10.1086/367622.

[9] F. Ahmad, D. Zhu, J. Sun, Environmental fate of tetracycline antibiotics: degradation pathway mechanisms, challenges, and perspectives, Environ. Sci. Eur. 33 (1) (2021) 64, https://doi.org/10.1186/s12302-021-00505-y.

[10] R. Daghrir, P. Drogui, Tetracycline antibiotics in the environment: a review, Environ. Chem. Lett. 11 (3) (2013) 209–227.

[11] M.S. de Ilurdoz, J.J. Sadhwani, J.V. Reboso, Antibiotic removal processes from water & wastewater for the protection of the aquatic environment - a review, J. Water Proc. Eng. 45 (2022) 102474, https://doi.org/10.1016/j.jwpe.2021.102474.

[12] M. Arabzadeh, Z. Eslamidoost, S. Rajabi, H. Hashemi, A. Aboulfotoh, F. Rosti, F. Nazari, B.P. Borj, M. Hajivand, Wastewater quality index (WWQI) as an indicator for the assessment of sanitary effluents from the oil and gas industries for reliable and sustainable water reuse, Groundwater for Sustainable Development (2023) 101015.

[13] M. Malakootian, A. Nasiri, M.R. Heidari, Removal of phenol from steel plant wastewater in three dimensional electrochemical (TDE) process using CoFe2O4@ AC/H2O2, Zeitschrift fur Physikalische Chemie 234 (10) (2020) 1661–1679, https://doi.org/10.1515/zpch-2019-1499.

[14] M. Pourshaban-Mazandarani, M. Ahmadian, A. Nasiri, A. Poormohammadi, CuCoFe2O4@AC magnetic nanocomposite as a novel heterogeneous Fenton-like nanocatalyst for Ciprofloxacin degradation from aqueous solutions, Appl. Water Sci. 13 (9) (2023), https://doi.org/10.1007/s13201-023-02002-4.

[15] M. Yazdani, A.A. Najafpoor, A.A. Dehghan, H. Alidadi, R. Zangi, S. Nourbakhsh, R. Ataei, Performance evaluation of combined ultrasonic/UV process in removal of tetracycline antibiotic from aqueous solutions using response surface methodology, Journal of Research in Environmental Health 3 (1) (2017) 11–20.

[16] A. Nasiri, F. Tamaddon, M.H. Mosslemin, M.A. Gharaghani, A. Asadipour, Magnetic nano-biocomposite CuFe2 O4 @methylcellulose (MC) prepared as a new nano-photocatalyst for degradation of ciprofloxacin from aqueous solution, Environmental Health Engineering and Management 6 (1) (2019) 39–41, https://doi.org/10.15171/EHEM.2019.05.

[17] A. Nasiri, M. Malakootian, M.R. Heidari, S.N. Asadzadeh, CoFe2O4@Methylcelloluse as a new magnetic nano biocomposite for sonocatalytic degradation of reactive blue 19, J. Polym. Environ. 29 (8) (2021) 2660–2675, https://doi.org/10.1007/s10924-021-02074-w.

[18] N. Golestani, A. Nasiri, M. Hashemi, CoFe2 O4 @MC/AC as an efficient and recyclable magnetic nanohybrid adsorbent for the metronidazole removal from simulated wastewater: bioassays and whole effluent toxicity, Desalination Water Treat. 280 (2022) 312–329, https://doi.org/10.5004/dwt.2022.29118.

[19] H.-Y. Chen, Y.-D. Liu, B. Dong, Biodegradation of tetracycline antibiotics in A/O moving-bed biofilm reactor systems, Bioproc. Biosyst. Eng. 41 (1) (2018) 47–56.

[20] S. Rajabi, A. Nasiri, M. Hashemi, Enhanced activation of persulfate by CuCoFe2O4@MC/AC as a novel nanomagnetic heterogeneous catalyst with ultrasonic for metronidazole degradation, Chemosphere 286 (Pt 3) (2022) 131872, https://doi.org/10.1016/j.chemosphere.2021.131872.

[21] F.-S. Tabatabai Yazdi, A. Ebrahimian Pirbazari, F. Esmaeili Khalil Saraei, N. Gilani, Investigation of photocatalytic performance of ternary nanocomposites (silver/titanium dioxide nanosheets/reduced graphene oxide) for degradation of tetracycline and modeling the process by ANFIS, Journal of Separation Science and Engineering 12 (2) (2021) 94–110, https://doi.org/10.22103/jsse.2021.2773.

[22] G. Yazdanpanah, M.R. Heidari, N. Amirmahani, A. Nasiri, Heterogeneous Sono-Fenton like catalytic degradation of metronidazole by Fe3O4@HZSM-5 magnetite nanocomposite, Heliyon 9 (6) (2023) e16461, https://doi.org/10.1016/j.heliyon.2023.e16461.

[23] I.R. Bautitz, R.F.P. Nogueira, Degradation of tetracycline by photo-Fenton process—solar irradiation and matrix effects, J. Photochem. Photobiol. Chem. 187 (1) (2007) 33–39.

[24] S. Chen, L. Tang, H. Feng, Y. Zhou, G. Zeng, Y. Lu, J. Yu, X. Ren, B. Peng, X. Liu, Carbon felt cathodes for electro-Fenton process to remove tetracycline via synergistic adsorption and degradation, Sci. Total Environ. 670 (2019) 921–931.

[25] S.H. Lin, R.S. Juang, Adsorption of phenol and its derivatives from water using synthetic resins and low-cost natural adsorbents: a review, J. Environ. Manag. 90 (3) (2009) 1336–1349, https://doi.org/10.1016/j.jenvman.2008.09.003.

[26] C. Gómez-Pacheco, M. Sánchez-Polo, J. Rivera-Utrilla, J. López-Peñalver, Tetracycline removal from waters by integrated technologies based on ozonation and biodegradation, Chem. Eng. J. 178 (2011) 115–121.

[27] M. Iqhrammullah, A. Fahrina, W. Chiari, K. Ahmad, F. Fitriani, N. Suriaini, E. Safitri, K. Puspita, Laccase immobilization using polymeric supports for wastewater treatment: a critical review, Macromol. Chem. Phys. 224 (9) (2023) 2200461.

[28] L. Hou, H. Zhang, L. Wang, L. Chen, Ultrasound-enhanced magnetite catalytic ozonation of tetracycline in water, Chem. Eng. J. 229 (2013) 577–584.

[29] G. Yazdanpanah, M.R. Heidari, A. Nasiri, Heterogeneous sono-fenton like catalytic degradation of metronidazole by Fe3O4@hzsm-5 magnetite nanocomposite, Heliyon 70 (4) (2023), https://doi.org/10.1002/jccs.202200514. In Press.

[30] N. Amirmahani, H. Mahdizadeh, N. Seyedi, A. Nasiri, G. Yazdanpanah, Synthesis and performance evaluation of chitosan/zinc oxide nanocomposite as a highly efficient adsorbent in the removal of reactive red 198 from water, J. Chin. Chem. Soc. 70 (4) (2023) 1–10, https://doi.org/10.1002/jccs.202200514.

[31] K. Adibkia, M. Barzegar Jalali, Y. Javadzadeh, R. Bayrami, G. Mohammadi, A review on the porous adsorbents in drug delivery systems, Pharmaceut. Sci. 18 (2) (2012) 103–118.

[32] N. Jaafarzadeh, M. Ahmadi, S. Silva Martinez, H. Amiri, Removal of as (III) and as (V) from aqueous solution using modified solid waste vegetable oil industry as a natural adsorbent, Environmental Engineering & Management Journal (EEMJ) 13 (2) (2014).

[33] N. Ballav, H.J. Choi, S.B. Mishra, A. Maity, Synthesis, characterization of Fe3O4@glycine doped polypyrrole magnetic nanocomposites and their potential performance to remove toxic Cr(VI), J. Ind. Eng. Chem. 20 (6) (2014) 4085–4093, https://doi.org/10.1016/j.jiec.2014.01.007.

[34] S. Goh, C.-h. Chia, S. Zakaria, M. Yusoff, C.Y. Haw, S. Ahmadi, H. Ming, H. Lim, Hydrothermal preparation of high saturation magnetization and coercivity cobalt ferrite nanocrystals without subsequent calcination, Mater. Chem. Phys. 120 (1) (2010) 31–35, https://doi.org/10.1016/j.matchemphys.2009.10.016.

[35] S. Maleky, A. Asadipour, A. Nasiri, R. Luque, M. Faraji, Tetracycline adsorption from aqueous media by magnetically separable Fe3O4@Methylcellulose/ APTMS: isotherm, kinetic and thermodynamic studies, J. Polym. Environ. 30 (8) (2022) 3351–3367, https://doi.org/10.1007/s10924-022-02428-y.

[36] A. Nasiri, M.R. Heidari, N. Javid, G. Yazdanpanah, New efficient and recyclable magnetic nanohybrid adsorbent for the metronidazole removal from simulated wastewater, J. Mater. Sci. Mater. Electron. 33 (33) (2022) 25103–25126, https://doi.org/10.1007/s10854-022-09216-3.

[37] A. Nasiri, M. Malakootian, N. Javid, Modelling and optimization of lead adsorption by CoFe2 O4 @CMC@HZSM-5 from aqueous solution using response surface methodology, Desalination Water Treat. 248 (2022) 134–148, https://doi.org/10.5004/dwt.2022.28046.

[38] A. Nasiri, M. Malakootian, M.A. Shiri, G. Yazdanpanah, M. Nozari, CoFe2O4@methylcellulose synthesized as a new magnetic nanocomposite to tetracycline adsorption: modeling, analysis, and optimization by response surface methodology, J. Polym. Res. 28 (5) (2021), https://doi.org/10.1007/s10965-021-02540-y.

[39] A. Nasiri, S. Rajabi, M. Hashemi, CoFe2O4@Methylcellulose/AC as a new, green, and eco-friendly nano-magnetic adsorbent for removal of reactive red 198 from aqueous solution, Arab. J. Chem. 15 (5) (2022), https://doi.org/10.1016/j.arabjc.2022.103745.

[40] K.S. Meera, D. Arunbabu, Magnetic cellulose green nanocomposite adsorbents for the removal of heavy metal ions in water/wastewater, in: Green Biopolymers and Their Nanocomposites, Springer, 2019, pp. 423–437.

[41] K. Ventura, R.A. Arrieta, M. Marcos-Hernández, V. Jabbari, C.D. Powell, R. Turley, A.W. Lounsbury, J.B. Zimmerman, J. Gardea-Torresdey, M.S. Wong, Superparamagnetic MOF@ GO Ni and Co based hybrid nanocomposites as efficient water pollutant adsorbents, Sci. Total Environ. (2020) 139–213.

[42] A. Benvidi, M. Yekrangi, S. Jahanbani, H.R. Zare, The extraction and measurement of nickel metal ion in crab, shellfish and rice samples using magnetic silk fibroin–EDTA ligand and furnace atomic absorption spectrometry, Food Chem. 319 (2020) 126–432.

[43] H.A.L. de Oliveira, A.F.C. Campos, G. Gomide, Y. Zhang, S. Ghoshal, Elaboration of a core@ shell bimagnetic nanoadsorbent (CoFe2O4@ γ-Fe2O3) for the removal of as (V) from water, Colloids Surf. A Physicochem. Eng. Asp. 600 (2020) 125002.

[44] F. Movahedi, A. Maghsodi, L. Adlnasab, Response surface methodology for heavy metals removal by tioglycolic-modified Zn–Fe layer double hydroxide as a magnetic recyclable adsorbent, Chem. Pap. 74 (9) (2020) 3169–3182, https://doi.org/10.1007/s11696-020-01149-7.

[45] A. Ghiasi, A. Malekpour, Octyl coated cobalt-ferrite/silica core-shell nanoparticles for ultrasonic assisted-magnetic solid-phase extraction and speciation of trace amount of chromium in water samples, Microchem. J. 154 (2020) 104–530.

[46] S.K. Sahoo, S. Padhiari, S. Biswal, B. Panda, G. Hota, Fe3O4 nanoparticles functionalized GO/g-C3N4 nanocomposite: an efficient magnetic nanoadsorbent for adsorptive removal of organic pollutants, Mater. Chem. Phys. 244 (2020) 122–710.

[47] T. Tang, S. Cao, C. Xi, X. Li, L. Zhang, G. Wang, Z. Chen, Chitosan functionalized magnetic graphene oxide nanocomposite for the sensitive and effective determination of alkaloids in hotpot, Int. J. Biol. Macromol. 146 (2020) 343–352, https://doi.org/10.1016/j.ijbiomac.2019.12.259.

[48] K.C. Das, B. Das, S.S. Dhar, Effective catalytic degradation of organic dyes by nickel supported on hydroxyapatite-encapsulated cobalt ferrite (Ni/HAP/CoFe 2 O 4) magnetic novel nanocomposite, Water, Air, Soil Pollut. 231 (2) (2020) 43.

[49] B. D'Cruz, M. Madkour, M.O. Amin, E. Al-Hetlani, Efficient and recoverable magnetic AC-Fe3O4 nanocomposite for rapid removal of promazine from wastewater, Mater. Chem. Phys. 240 (2020) 122109, https://doi.org/10.1016/j.matchemphys.2019.122109.

[50] A. Nasiri, S. Rajabi, M. Hashemi, H. Nasab, CuCoFe2O4@MC/AC as a new hybrid magnetic nanocomposite for metronidazole removal from wastewater: bioassay and toxicity of effluent, Separ. Purif. Technol. 296 (2022), https://doi.org/10.1016/j.seppur.2022.121366.

[51] N. Amirmahani, H. Mahdizadeh, N. Seyedi, A. Nasiri, G. Yazdanpanah, Synthesis and performance evaluation of chitosan/zinc oxide nanocomposite as a highly efficient adsorbent in the removal of reactive red 198 from water, J. Chin. Chem. Soc. 70 (4) (2023) 869–878, https://doi.org/10.1002/jccs.202200514.

[52] R. Rahmi, L. Lelifajri, F. Fathurrahmi, H. Fathana, M. Iqhrammullah, Preparation and characterization of PEGDE-EDTA-modified magnetic chitosan microsphere as an eco-friendly adsorbent for methylene blue removal, S. Afr. J. Chem. Eng. 43 (2023) 296–302.

[53] W.S. Wan Ngah, L.C. Teong, M.A.K.M. Hanafiah, Adsorption of dyes and heavy metal ions by chitosan composites: a review, Carbohydr. Polym. 83 (4) (2011) 1446–1456, https://doi.org/10.1016/j.carbpol.2010.11.004.

[54] J.H. Chen, H. Lin, Z.H. Luo, Y.S. He, G.P. Li, Cu (II)-imprinted porous film adsorbent Cu–PVA–SA has high uptake capacity for removal of Cu (II) ions from aqueous solution, Desalination 277 (1–3) (2011) 265–273.

[55] N. Xiao, L. Wang, H. Wang, S. Wang, T. Zhu, Electron-withdrawing/donating groups (EWG/EDG) modified graphene oxide-oxidized-multiwalled carbon nanotubes and these performances in electrochemistry and adsorption, J. Electroanal. Chem. 895 (2021) 115450.

[56] M. Malakootian, A. Nasiri, A. Asadipour, E. Kargar, New magnetic nanophotocatalyst CoFe2O4@CMC as a new magnetic nanophotocatalyst for ciprofloxacin degradation from aqueous media, Process Saf. Environ. Protect. 129 (2019) 138–151, https://doi.org/10.1016/j.psep.2019.06.022.

[57] M. Malakootian, A. Nasiri, H. Mahdizadeh, Metronidazole adsorption on CoFe2O4/activated carbon@chitosan as a new magnetic biocomposite: modelling, analysis, and optimization by response surface methodology, Desalination Water Treat. 164 (2019) 215–227, https://doi.org/10.5004/dwt.2019.24433.

[58] F. Tamaddon, M.H. Mosslemin, A. Asadipour, M.A. Gharaghani, A. Nasiri, Microwave-assisted preparation of ZnFe2O4@methyl cellulose as a new nano-biomagnetic photocatalyst for photodegradation of metronidazole, Int. J. Biol. Macromol. 154 (2020) 1036–1049, https://doi.org/10.1016/j.ijbiomac.2020.03.069.

[59] R. Rahmi, L. Lelifajri, M. Iqbal, F. Fathurrahmi, J. Jalaluddin, R. Sembiring, M. Farida, M. Iqhrammullah, Preparation, characterization and adsorption study of PEDGE-cross-linked magnetic chitosan (PEDGE-MCh) microspheres for Cd2+ removal, Arabian J. Sci. Eng. 48 (1) (2023) 159–167, https://doi.org/10.1007/s13369-022-06786-6.

[60] Julinawati Rahmi, M. Nina, H. Fathana, M. Iqhrammullah, Preparation and characterization of new magnetic chitosan-glycine-PEGDE (Fe3O4/Ch-G-P) beads for aqueous Cd(II) removal, J. Water Proc. Eng. 45 (2022) 102493, https://doi.org/10.1016/j.jwpe.2021.102493.

[61] M. Rahmi, U. Iqhrammullah, H. Husin Audina, H. Fathana, Adsorptive removal of Cd (II) using oil palm empty fruit bunch-based charcoal/chitosan-EDTA film composite, Sustainable Chemistry and Pharmacy 21 (2021) 100449, https://doi.org/10.1016/j.scp.2021.100449.

[62] G. Oliveira, G. Filho, J. Vieira, R. Assunção, C. Meireles, D. Cerqueira, R. Oliveira, W. Silva, L. Motta, Synthesis and application of methylcellulose extracted from waste newspaper in CPV-ari portland cement mortars, J. Appl. Polym. Sci. 118 (2010) 1380–1385, https://doi.org/10.1002/app.32477.

[63] R.L. Oliveira, J.G. Vieira, H.S. Barud, R. Assunção, G. R Filho, S.J. Ribeiro, Y. Messadeqq, Synthesis and characterization of methylcellulose produced from bacterial cellulose under heterogeneous condition, J. Braz. Chem. Soc. 26 (2015) 1861–1870.

[64] M.F. Queiroz, K.R. Teodosio Melo, D.A. Sabry, G.L. Sassaki, H.A.O. Rocha, Does the use of chitosan contribute to oxalate kidney stone formation? Mar. Drugs 13 (1) (2014) 141–158.

[65] M. Mallapur, P. Shaikh, R. Kambale, H. Jamadar, B. Chougule, Structural and electrical properties of nanocrystalline cobalt substituted nickel zinc ferrite, J. Alloys Compd. 479 (1–2) (2009) 797–802.

[66] A.M. El-Sayed, Influence of zinc content on some properties of Ni-Zn ferrites, Ceram. Int. 28 (4) (2002) 363–367, https://doi.org/10.1016/S0272-8842(01)00103-1.

[67] M.M. Mallapur, P. Shaikh, R. Kambale, H.V. Jamadar, P.U. Mahamuni, B.K. Chougule, Structural and electrical properties of nanocrystalline cobalt substituted nickel zinc ferrite, Journal of Alloys and Compounds - J ALLOYS COMPOUNDS 479 (1–2) (2009) 797–802, https://doi.org/10.1016/j.jallcom.2009.01.142.

[68] L. McCusker, IUPAC nomenclature for ordered microporous and mesoporous materials and its application to non-zeolite microporous mineral phases, Reviews in Mineralogy & Geochemistry - REV MINERAL GEOCHEM 57 (1) (2005) 1–16, https://doi.org/10.2138/rmg.2005.57.1.

[69] Y. Guo, W. Huang, B. Chen, Y. Zhao, D. Liu, Y. Sun, B. Gong, Removal of tetracycline from aqueous solution by MCM-41-zeolite A loaded nano zero valent iron: synthesis, characteristic, adsorption performance and mechanism, J. Hazard Mater. 339 (2017) 22–32, https://doi.org/10.1016/j.jhazmat.2017.06.006.

[70] J. He, F. Ni, A. Cui, X. Chen, S. Deng, F. Shen, C. Huang, G. Yang, C. Song, J. Zhang, D. Tian, L. Long, Y. Zhu, L. Luo, New insight into adsorption and co-adsorption of arsenic and tetracycline using a Y-immobilized graphene oxide-alginate hydrogel: adsorption behaviours and mechanisms, Sci. Total Environ. 701 (2020) 134363, https://doi.org/10.1016/j.scitotenv.2019.134363.

[71] E. Çalışkan, S. Göktürk, Adsorption characteristics of sulfamethoxazole and metronidazole on activated carbon, Separ. Sci. Technol. 45 (2) (2010) 244–255.

[72] H. Luo, Y. Liu, H. Lu, Q. Fang, H. Rong, Efficient adsorption of tetracycline from aqueous solutions by modified alginate beads after the removal of Cu (II) ions, ACS Omega 6 (9) (2021) 6240–6251.

[73] T. Ahamad, M. Naushad, T. Al-Shahrani, N. Al-Hokbany, S.M. Alshehri, Preparation of chitosan based magnetic nanocomposite for tetracycline adsorption: kinetic and thermodynamic studies, Int. J. Biol. Macromol. 147 (2020) 258–267, https://doi.org/10.1016/j.ijbiomac.2020.01.025.

[74] R. Kasraei, M. Malakootian, Tetracycline adsorption from aqueous solutions by a magnetic nanoadsorbent modified with ionic liquid, Desalination Water Treat. 209 (2021) 289–301.

[75] M. Ahmad, T. Nawaz, M.M. Alam, Y. Abbas, S. Ali, M. Imran, S. Zhang, Z. Wu, Effective poly (Cyclotriphosphazene-co-4,4′-sulfonyldiphenol)@rgo sheets for tetracycline adsorption: fabrication, characterization, adsorption kinetics and thermodynamics, Nanomaterials 11 (6) (2021), https://doi.org/10.3390/nano11061540.

[76] F. Batool, J. Akbar, S. Iqbal, S. Noreen, S.N.A. Bukhari, Study of isothermal, kinetic, and thermodynamic parameters for adsorption of cadmium: an overview of linear and nonlinear approach and error analysis, Bioinorgan. Chem. Appl. 2018 (2018) 3463724, https://doi.org/10.1155/2018/3463724.

[77] N. Nasseh, B. Barikbin, L. Taghavi, M.A. Nasseri, Adsorption of metronidazole antibiotic using a new magnetic nanocomposite from simulated wastewater (isotherm, kinetic and thermodynamic studies), Compos. B Eng. 159 (2019) 146–156.

[78] J.A. Pellicer, M.I. Rodríguez-López, M.I. Fortea, J.A. Gabaldón Hernández, C. Lucas-Abellán, M.T. Mercader-Ros, A. Serrano-Martínez, E. Núñez-Delicado, P. Cosma, P. Fini, E. Franco, R. García, M. Ferrándiz, E. Pérez, M. Ferrándiz, Removing of Direct Red 83:1 using α- and HP-α-CDs polymerized with epichlorohydrin: kinetic and equilibrium studies, Dyes Pigments 149 (2018) 736–746, https://doi.org/10.1016/j.dyepig.2017.11.032.

[79] M. Malakootian, M. Hashemi, A. Toolabi, A. Nasiri, Investigation of nickel removal using poly (amidoamine) generation 4 dendrimer (PAMAM G4) from aqueous solutions, Journal of Engineering Research 6 (2) (2018).

[80] W.J. Weber Jr., J.C. Morris, Closure to "Kinetics of Adsorption on Carbon from solution", J. Sanit. Eng. Div. 89 (6) (1963) 53–55.

[81] S. Maleky, A. Asadipour, A. Nasiri, R. Luque, M. Faraji, Tetracycline adsorption from aqueous media by magnetically separable Fe3O4@ methylcellulose/APTMS: isotherm, kinetic and thermodynamic studies, J. Polym. Environ. (2022) 1–17.

[82] J. Zhang, M.A. Khan, M. Xia, A.M. Abdo, W. Lei, C. Liao, F. Wang, Facile hydrothermal synthesis of magnetic adsorbent CoFe2O4/MMT to eliminate antibiotics in aqueous phase: tetracycline and ciprofloxacin, Environ. Sci. Pollut. Control Ser. 26 (1) (2019) 215–226, https://doi.org/10.1007/s11356-018-3452-6.

[83] B. Yu, Y. Bai, Z. Ming, H. Yang, L. Chen, X. Hu, S. Feng, S.-T. Yang, Adsorption behaviors of tetracycline on magnetic graphene oxide sponge, Mater. Chem. Phys. 198 (2017) 283–290.

[84] I. Turku, T. Sainio, E. Paatero, Thermodynamics of tetracycline adsorption on silica, Environ. Chem. Lett. 5 (4) (2007) 225–228.

[85] H. Wang, Y. Chu, C. Fang, F. Huang, Y. Song, X. Xue, Sorption of tetracycline on biochar derived from rice straw under different temperatures, PLoS One 12 (8) (2017) e0182776.

[86] A.H. Nezhad, M. Khodadadi, N. Nasseh, Investigation of the efficiency of powdered and granular magnetic activated carbon nano composites for the adsorption of metronidazole from aqueous solutions (isotherms and kinetics study), Desalination Water Treat. (2020) 198.

[87] B. Kakavandi, R.R. Kalantary, A.J. Jafari, A. Esrafily, A. Gholizadeh, A. Azari, Efficiency of powder activated carbon magnetized by Fe3O4 nanoparticles for amoxicillin removal from aqueous solutions: equilibrium and kinetic studies of adsorption process, Iran. J. Health Environ. 7 (2014) 21–34.

[88] A. Fatemeh, M. Gholami, A. Jonidi jafari, M. Kermani, H. Asgharnia, R. RezaeiKalantari, Study of tetracycline and metronidazole adsorption on biochar prepared from rice bran kinetics, isotherms and mechanisms, Desalination Water Treat. 159 (2019) 390–401, https://doi.org/10.5004/dwt.2019.24140.

[89] X. Weng, W. Cai, G. Owens, Z. Chen, Magnetic iron nanoparticles calcined from biosynthesis for fluoroquinolone antibiotic removal from wastewater, J. Clean. Prod. 319 (2021) 128734, https://doi.org/10.1016/j.jclepro.2021.128734.

[90] M. Kumari, R.B. Sunoj, P.V. Balaji, Exploration of CH center dot center dot center dot center dot pi mediated stacking interactions in saccharide: aromatic residue complexes through conformational sampling, Carbohydr. Res. 361 (2012) 133–140.

[91] J.L. Asensio, A. Ardá, F.J. Cañada, J. Jimenez-Barbero, Carbohydrate–aromatic interactions, Accounts Chem. Res. 46 (4) (2013) 946–954.

[92] M. Nishio, The CH/π hydrogen bond in chemistry. Conformation, supramolecules, optical resolution and interactions involving carbohydrates, Phys. Chem. Chem. Phys. 13 (31) (2011) 13873–13900.